Continental subduction recorded by Neoproterozoic eclogite and garnet amphibolites from Western Hoggar (Tassendjanet terrane, Tuareg Shield, Algeria)

Julien Berger, Khadidja Ouzegane, Abderrahmane Bendaoud, Jean-Paul Liegeois, Jean-Robert Kienast, Olivier Bruguier, Renaud Caby

Continental subduction recorded by Neoproterozoic eclogite and garnet amphibolites from Western Hoggar (Tassendjanet terrane, Tuareg Shield, Algeria)

Julien Berger[a,b,*], Khadidja Ouzegane[c], Abderrahmane Bendaoud[c], Jean-Paul Liégeois[d], Jean-Robert Kiénast[e], Olivier Bruguier[f], Renaud Caby[f]

[a] *Géosciences Environnement Toulouse, Université Paul Sabatier, 31400 Toulouse, France*
[b] *Geological Institute, ETH Zürich, 8092 Zürich, Switzerland*
[c] *Department of Geology, Université des Sciences et Techniques Houari Boumediene, 16111 Algiers, Algeria*
[d] *Geodynamics and Mineral Resources, Royal Museum for Central Africa, 3080 Tervuren, Belgium*
[e] *IPGP, 1 rue Jussieu, 75238-Paris Cedex 05, France*
[f] *Géosciences Montpellier, Université de Montpellier 2, 34095 Montpellier, France*

Neoproterozoic eclogite and garnet amphibolites, representing retrogressed eclogites, from the Tassendjanet-Tidéridjaouine terrane in the Pan-African Western Hoggar (Tuareg shield, Southern Alge-ria) form lenses enclosed in 1.8 Ga subalkaline Paleoproterozoic orthogneisses. They lie along a major sinistral shear zone marking the boundary with the Archean/Paleoproterozoic granulitic In Ouzzal ter-rane and are associated with high-pressure metasediments. According to thermodynamic calculations, peak condition of the eclogitic stage is 650 °C, 20–22 kbar followed by post-peak heating and exhumation at 730 °C, 10–14 kbar and cooling to 610 °C, 7–10 kbar. Their major, trace-element and isotopic compo-sitions are consistent with emplacement of former basalts in the shoulder of a 700–800 Ma continental rift that evolved to an oceanic basin. The eclogite and garnet amphibolites were thus part of the conti-nental portion of a subducting slab that was pulled down by a denser oceanic lithosphere. Sheath and recumbent folds associated with the exhumation of HP units are verging toward the west, meaning that the former slab was dipping to the east. U–Pb zircon dating on metamorphic zircons bordering ilmenite and rutile in the eclogite gave an age of 623 ± 2 Ma, interpreted as the syn-collisional exhumation stage of the high-pressure unit. This event was rapidly followed by transpressional tectonics and abundant magmatism linked to the northward motion of the adjacent In Ouzzal terrane.

1. Introduction

Eclogites, blueschists and high-pressure (HP) metasediments are a common feature of Phanerozoic and especially peri-Mediterranean alpine belts. They are formed in subducting slabs either of continental or oceanic affinity. Exhumation of the HP units is a tricky process, especially if the slab is oceanic with a crustal section dominated by dense basaltic rocks. The density of an eclogite is close or higher than surrounding mantle rocks at lithostatic pressures corresponding to HP metamorphism (>14 kbar); it usually precludes an exhumation controlled by buoyancy forces only. Subducted continental margins are dominated by felsic material whose density is always lower than mantle rocks at pressure at which HP rocks form. The exhumation of continental units is therefore at least partly driven by their positive buoyancy (Chemenda et al., 1996; Ernst et al., 1997). Exhumation of both continental and oceanic slabs is also controlled or facilitated by early-orogenic tectonics and erosion (see Guillot et al., 2009), slab eduction following detachment (Duretz et al., 2012), flow within a weak subduction channel above the plunging slab (Gerya et al., 2002; Guillot et al., 2009), or corner flow (Burov et al., 2001). Each process occurs at different depth (Burov et al., 2001). UHP units are thus mostly of continental origin because they have a positive buoyancy (Chopin, 2003) that lead to fast exhumation from great depths. In contrast, most oceanic eclogites did not record pressures higher than 20–23 kbar (Agard et al., 2009).

* Corresponding author at: Géosciences Environnement Toulouse, 14, Avenue Edouard Belin, 31400 Toulouse, France. Tel.: +33 0 5 61 33 26 31.
E-mail address: julien.berger@get.obs-mip.fr (J. Berger).

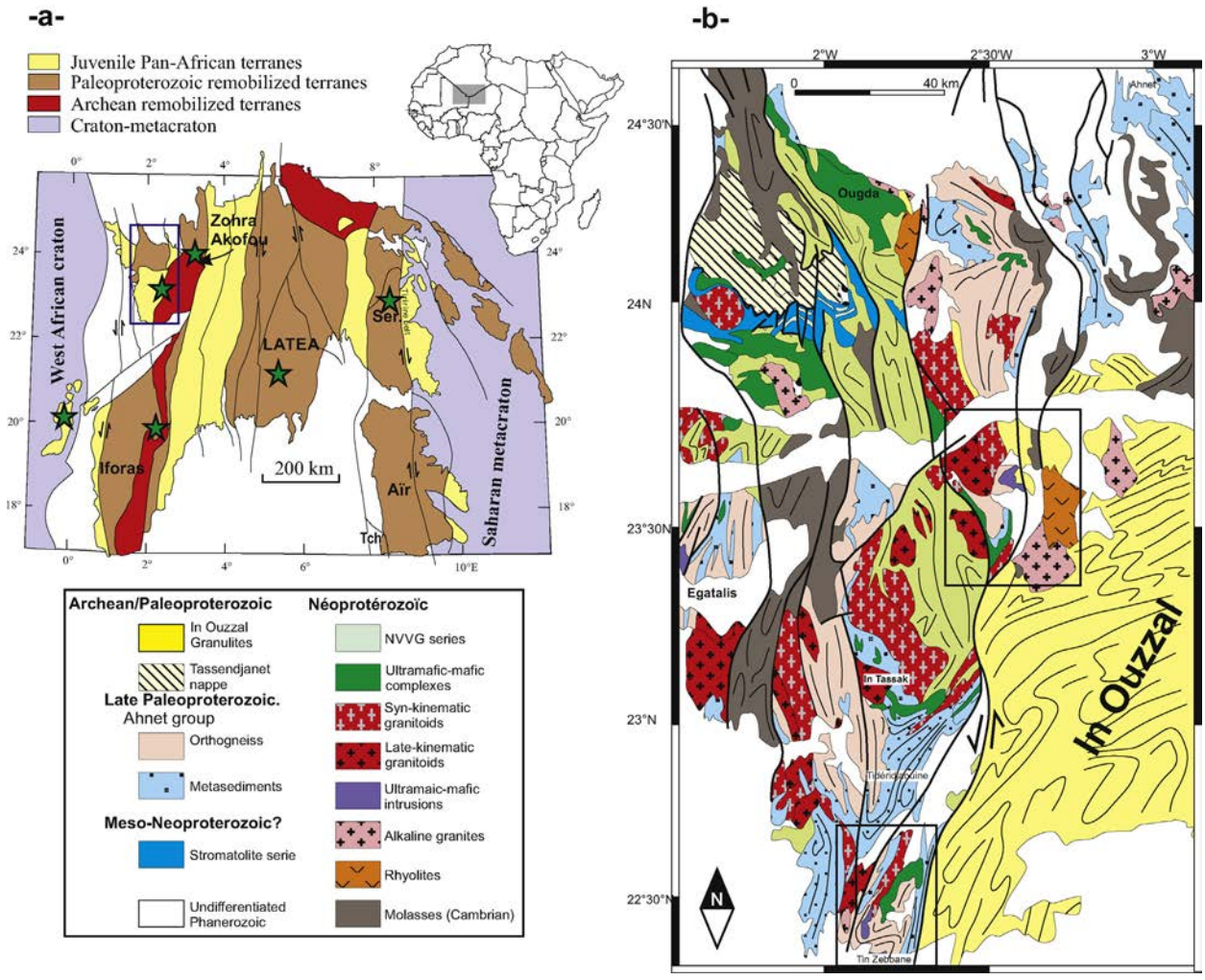

Fig. 1. Simplified geological maps of the Tuareg Shield (a) and the Tassenjanet-Tideridjaouine-Ahnet-In Ouzzal area. Modified after Black et al. (1994) (a) and Caby (1969)(b). The stars in map (a) show the location of high-pressure units. Ser.: Serouenout oceanic terrane, Zorha and Akofou: camp Zohra complex and Akofou andesites.

The existence of subduction in the Early Earth is much more controversial. Preserved HP-LT rocks before the Neoproterozoic are scarce (Cawood et al., 2006; Mints et al., 2010; Ganne et al., 2012) meaning that subduction probably existed but also that subducted units were more difficult to exhume or to preserve in hot and light Early Earth mantle. There is now a consensus on the idea that modern style plate tectonics exist at least since the Neoproterozoic as evidenced by the occurrences of ophiolites, eclogites and other HP metamorphic rocks (Stern, 2005). Neoproterozoic HP units are however rare, except in Pan-African belts (Agbossoumondé et al., 2001; Jahn et al., 2001; John et al., 2003; Boniface and Schenk, 2012) but growing evidences suggest that processes forming HP-LT units were the same that in modern Earth. Neoproterozoic eclogites are abundant in the Tuareg Shield (Algeria, Mali and Niger, see Fig. 1a), an area mainly structured during the Pan-African orogenic event (Black et al., 1994). They occur along former major thrusts in the Central Hoggar (LATEA, Sautter, 1985; Bernard-Griffiths et al., 1991; Liégeois et al., 2003; Zetoutou et al., 2004), in the Serouenout oceanic terrane (Bittam-Derridj et al., 2010), along the West Ouzzalian Shear Zone in the Western Hoggar (Caby and Monié, 2003) and in the Adrar des Iforas some garnet amphibolites may represent retrogressed eclogites along the same shear zone (Champenois et al., 1987).

The age of high-pressure metamorphism in Hoggar is not well established. ^{39}Ar–^{40}Ar laser dating on phengites from the Tidéridjaouine garnet-kyanite-phengite metasediments yielded ages down to 620 Ma (Caby and Monié, 2003). Garnet amphibolites from the central Hoggar were dated by Sm–Nd mineral isochrons (Liégeois et al., 2003), the oldest age obtained is 680 Ma but these samples show many evidences for isotopic and metamorphic re-equilibration after HP crystallization. This means that the process of accretion of the western Tuareg terranes during the Pan-African orogeny is still poorly constrained.

This paper presents petrological, geochemical and geochronological investigations on the eclogite and garnet amphibolites reported by Caby and Monié (2003) to better define: (i) the *P*–*T* conditions and the dynamics of the fossil subduction zone; (ii) the composition and tectonic setting of their magmatic precursor as well as (iii) the age of HP event and the geodynamic evolution of Western Hoggar.

2. Geological setting

The Tuareg shield, in which is included Hoggar (southern Algeria), is composed of both juvenile Neoproterozoic terranes and Archean/Paleoproterozoic blocks (Fig. 1) variably remobilized during the Pan-African orogeny (Black et al., 1994; Caby, 2003; Liégeois et al., 2003). The later Variscan and Alpine orogeny had no major imprint on the structure of the area, they were limited to open folding in the Early Permian (Haddoum et al., 2001) and uplift in

the Cenozoic (Rougier et al., 2013). Terranes were assembled during the Pan-African orogeny *sensu lato*, but the collage occurred in several steps. In the Western Hoggar, collision with the West African craton (WAC) occurred just after or during continental subduction of the WAC passive margin. In the Gourma belt, the high-pressure metamorphism affecting the WAC passive margin is dated at 620 ± 13 Ma (^{147}Sm–^{143}Nd mineral isochron on eclogite; Jahn et al., 2001) and 623 ± 3 Ma (^{39}Ar–^{40}Ar dating on phengite from HP metasediments; Jahn et al., 2001).

The eclogites from this study have been sampled in the Tassendjanet-Tidéridjaouine terrane (TTt) close to the sinistral West Ouzzalian Shear Zone, marking the sharp boundary with the Archean/Paleoproterozoic In Ouzzal ultrahigh-temperature (UHT) terrane (Caby, 1996; Ouzegane et al., 2003), only affected by brittle deformation during the Pan-African orogeny (Fig. 1). The TTt is formed in the north by several high crustal level units (Fig. 1): (i) the Tassendjanet Nappe, involving the Paleoproterozoic Tassendjanet basement (Allègre and Caby, 1972; Caby and Monié, 2003) and its carbonate cover with stromatolite-bearing horizons of assumed late Mesoproterozoic age (by comparison with the c. 1100 Ma Atar Group, see Caby and Monié, 2003; Rooney et al., 2010); (ii) a complex Neoproterozoic arc terrane (the Ougda complex, Dostal et al., 1996) rooted by gabbro-dioritic arc plutons that intruded in part the carbonate cover, which in turn was unconformably overlain by ≥6000 m of andesite flows and volcanic greywackes (Tassendjanet/Akofou complex). The southern part of TTt consists of deeper crustal levels of the Pan-African belt affected by large scale recumbent folding generated under amphibolite facies metamorphism of high-pressure affinity (Caby and Monié, 2003). The oldest rocks from this metamorphic belt labelled here the Ahnet-Tidéridjaouine Group (ATG) (Figs. 1 and 2), affected by the Pan-African events only, consists of orthoquartzites, aluminous schists and orthogneisses derived from granites and subalkaline and alkaline rhyolites dated at 1.75 Ga (Statherian age; Caby and Andreopoulos-Renaud, 1983; Dostal et al., 1979; Caby, 2003). A younger paraconformable group of quartzites and carbonates correlated with the carbonates of the Tassendjanet Nappe overlies the ATG both in the Ahnet and in the Tidéridjaouine areas (Moussine-Pouchkine et al., 1988). Pre-metamorphic Neoproterozoic magmatism in NW Hoggar includes a mafic sill complex emplaced in the carbonate cover of the Tassendjanet domain such as that of the Ougda complex (Fig. 1) emplaced around 680 Ma (^{39}Ar–^{40}Ar cooling age, Caby and Monié, 2003). The Neoproterozoic volcanic-volcaniclastic Group (NVVG) (Fig. 1) was deposited after 680 Ma onto older metasedimentary rocks and the Ougda mafic rocks (Caby and Monié, 2003). It is mainly composed of a huge monotonous formation of turbiditic greywackes and conglomerates formed by the erosion of calc-alkaline lavas and plutons ranging from basaltic andesites to dacites in composition (Caby et al., 1977; Chikhaoui et al., 1978).

The eclogites have been sampled at two locations (Table 1): Tiléouine (Fig. 2a) and Tidéridjaouine (Fig. 2b). The Tiléouine samples are mainly retrogressed eclogites (garnet amphibolites) forming small lenses (max. 20 m thick) inserted in subalkaline orthogneiss adjacent to muscovite metaquartzites (Fig. 2a). All rocks were affected by west-verging recumbent to sheath folds coeval with a prominent SE-dipping streaky lineation. Compositional banding of the mafic rock is depicted by garnet-bearing centimetre-thick layers, from which was found one sample of kyanite eclogite (<1 cm thick layer) reported by Caby and Monié (2003). Interestingly the main lens displays rather sharp contact with the sub-alkaline gneisses, suggesting that the protolith could represent a dike or a sill, whereas other lenses show gradational contacts with amphibole-rich, fluorite-bearing alkaline orthogneiss that apparently did not registered HP conditions. The Tiléouine domain represents the southern extremity of the Pan-African middle crustal block that was extruded obliquely northward and expelled from the edge or from below of the Paleoproterozoic In Ouzzal Granulitic terrane (Caby, 2003). The domain is separated from the greenschist facies metagreywackes of the NVVG group, to the west, by a late strike-slip shear zone (Fig. 2a).

The Tidéridjaouine eclogites and garnet amphibolites are sandwiched in two-mica migmatitic metasediments along N60-elongated lenses (Fig. 2b). Close to this eclogite occurrence, the Tidéridjaouine HP metasediments represented by kyanite-phengite-garnet bearing quartz-rich and quartz-poor metapelites (Caby and Monié, 2003) are exposed. ^{39}Ar–^{40}Ar laser dating in the core of phengite from HP metasediments yielded ages around 620–615 Ma, which were interpreted as cooling age after exhumation rather than dating the HP metamorphism (Caby and Monié, 2003).

3. Petrographic descriptions and mineral chemistry

3.1. Tidéridjaouine

Ten eclogites/garnet amphibolites were sampled and 4 were selected for detailed mineralogical and geochemical investigations. The eclogite TINZ 3 (Fig. 3a) consists of 40 vol.% of polygonal omphacite, 55 vol.% of round garnet and 5 vol% of rutile and ilmenite. Round omphacite (~500 μm) is well preserved but has quite low jadeite contents (Fig. 4a) from 12 to 20 mol%; Mg#: 77–86), the most Na-rich pyroxene (corresponding to a Na_2O content of 3.1 wt%) forming small inclusions into garnet. Garnet forms xenoblastic to idioblastic grains ranging from 0.5 to 1 mm wide, with an inner core containing inclusions of omphacite, rutile, apatite and zircon (up to 40 μm in length) and quartz in the innermost core. Core compositions are homogeneous ($Alm_{49-50}Prp_{27-28}Grs_{20-21}Spss_{1-2}$). Zoning profile (Fig. 4b) is characterized by a small increase in Fe content (up to 52 Alm mol%) accompanied by a decrease of Ca (down to 16 mol% Grs) toward the rim with an external most rim enriched in Mg but depleted in Fe ($Alm_{49-50}Prp_{31}Grs_{20}Spss_{1}$). The eclogite shows minor development of retrograde assemblage (<3 vol.%), represented by hornblende (Mg#: 69–77; Si: 6.3–6.6 a.p.f.u.)–plagioclase (An_{33-45}) coronas around garnet grains (Fig. 5).

Garnet amphibolites show different petrographical features following the degree of retrogression after the eclogite stage. Some samples (TINZ 4 and TINZ 5) have preserved direct evidence of eclogite-facies assemblages, omphacite is indeed replaced by fine symplectitic intergrowths (Fig. 3b) of more or less sodic diopside (8–15 mol% jadeite, Fig. 4a) with plagioclase (An_{20-40}). Garnet from sample TINZ 4 has similar composition than the eclogite TINZ 3 (Fig. 4c). Amphibole–plagioclase–quartz intergrowths partly replace garnet at its rim, it is a magnesiohastingsite in sample TINZ 5 and a tschermakite in sample TINZ 4 (Fig. 5a). The last studied sample TINZ 1 is a garnet amphibolite with green brown polygonal tschermakite (Mg#: 44–55, Si: 6.2–6.5 a.p.f.u.), xenomorphic garnet ($Alm_{62-65}Prp_{7-10}Grs_{23-27}Spss_{1-3}$) partly destabilized into amphibole–plagioclase–quartz assemblages and polygonal plagioclase (An_{20-25}). No evidence for eclogitic assemblage is preserved in this sample. Accessory phases include rutile, ilmenite, titanite, apatite and zircon (up to 10 μm in length) included into garnet or bordering ilmenite.

3.2. Tiléouine

All samples from Tiléouine are garnet amphibolites either having preserved diopside–plagioclase symplectite after omphacite or not. Porphyroclastic kyanite has also been reported by Caby and Monié (2003) at a close locality from one preserved eclogite but it

Table 1
UTM WGS 84 (zone 31Q) coordinates and main petrographic characteristics of the studied samples.

	UTM X	UTM Y	Eclogitic stage	Anhydrous retrograde	Hydrous retrograde
Til 4	449058	2601724	grt	Pl-di	Amph-pl-ep-ilm
Til 6	449058	2601724	grt		Amph-pl-ep-ilm
Til 9	449058	2601724	grt		Amph-pl-ilm
Tinz 1	416115	2503825	grt	Pl-di	Amph-pl-ep-ilm-ttn
Tinz 3	416342	2504026	Omph, grt, rutile, q		Amph-pl-ilm
Tinz 4	415965	2503927	grt	Pl-di	Amph-pl-ep-ilm-ttn
Tinz 5	416000	2503960	grt	Pl-di	Amph-pl-ep-ilm-ttn

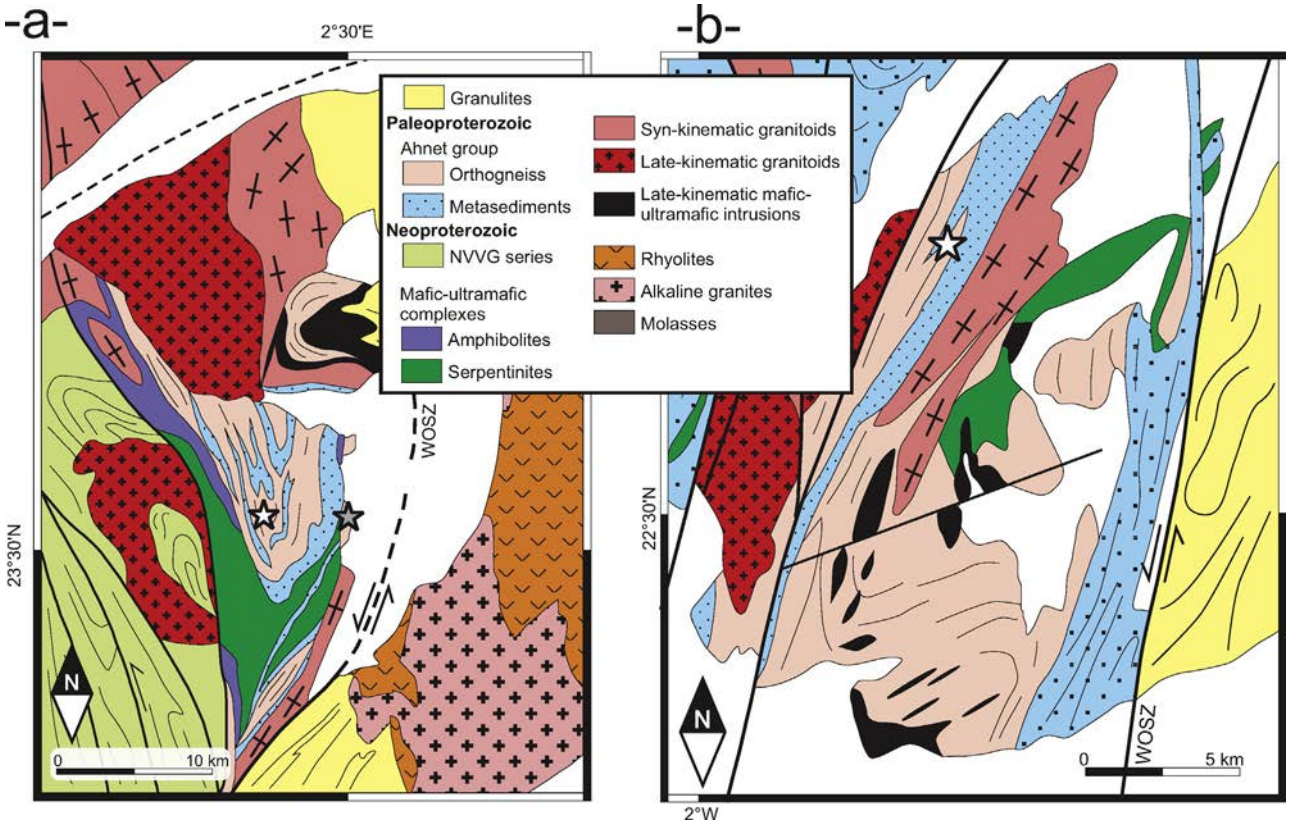

Fig. 2. Geological map of the Tiléouine (a) and Tidéridjaouine-Tin Zebbane (b) areas, modified after Caby (1969). The grey star shows the location of the kyanite eclogite reported by Caby and Monié (2003) and the white stars indicate the position of the eclogite and garnet amphibolite samples used in the present study. WOSZ: West In Ouzzal Shear Zone.

was not found in our samples. In sample TIL 4, sodic diopside (up to 10 jadeite mol%, Fig. 4a) is preserved in fine intergrowths with plagioclase (An_{18-20}). Round porphyroclastic garnet (comparable in composition to garnet from TINZ 1) is zoned (Fig. 4d) with core composition being richer in Mn ($Alm_{61-63}Prp_{4-6}Grs_{30}Spss_{2-6}$) and the rim enriched in Ca and Mg ($Alm_{61-62}Prp_{6-9}Grs_{30-32}Spss_{0-1}$). It is rich in inclusions of quartz, plagioclase and amphibole. Garnet is surrounded by plagioclase-amphibole-quartz intergrowths and coarse amphibole (low-Na magnesiohornblende) blasts grew at the expense of plagioclase–diopside symplectite. The two other samples (TIL 6 and TIL 9) have the same petrological and mineralogical characteristics: round zoned garnet (same composition and zoning profile than TIL 4) surrounded by Na-rich (up to 2.6 wt% Na_2O) amphibole, plagioclase (An_{35-42}) and quartz intergrowths; magnesiohornblende–plagioclase symplectites after omphacite and zoned amphibole blasts (Fig. 5a and b) showing a brown-green core (magnesiohornblende) and a blue-green rim (Na-bearing tschermakite, up to 2 wt% Na_2O) in close contact with epidote. Minute amphibole neoblast in epidote-bearing and plagioclase-free microdomains also shows high content in the edenitic end-member (up to 0.6 Na per formula unit in A site, Fig. 5b). Accessory phases are micro-zircon (<10 μm large), apatite, titanite and ilmenite.

4. Thermobarometry and fixed-composition phase diagrams

4.1. Eclogite-facies metamorphism

The absence of kyanite in the eclogite TINZ 3 does not allow an independent estimate of pressure and temperature. The garnet-clinopyroxene geothermometer of Ravna (2000) has been used to estimate the equilibrium temperature of the omphacite–garnet pairs. Two assemblages were used for calculations: (i) composition of omphacitic inclusions into garnet and the core composition of the latter; (ii) omphacite from the matrix and adjacent garnet rim. Results obtained are similar for both assemblages: a temperature range of 580–660 °C with a mean at 630 °C (for a pressure fixed at 20 kbar, the temperature dependence on pressure being 2.5 °C/kbar).

The PT evolution of the eclogite was investigated using *P–T* phase diagram for a fixed composition corresponding to the bulk

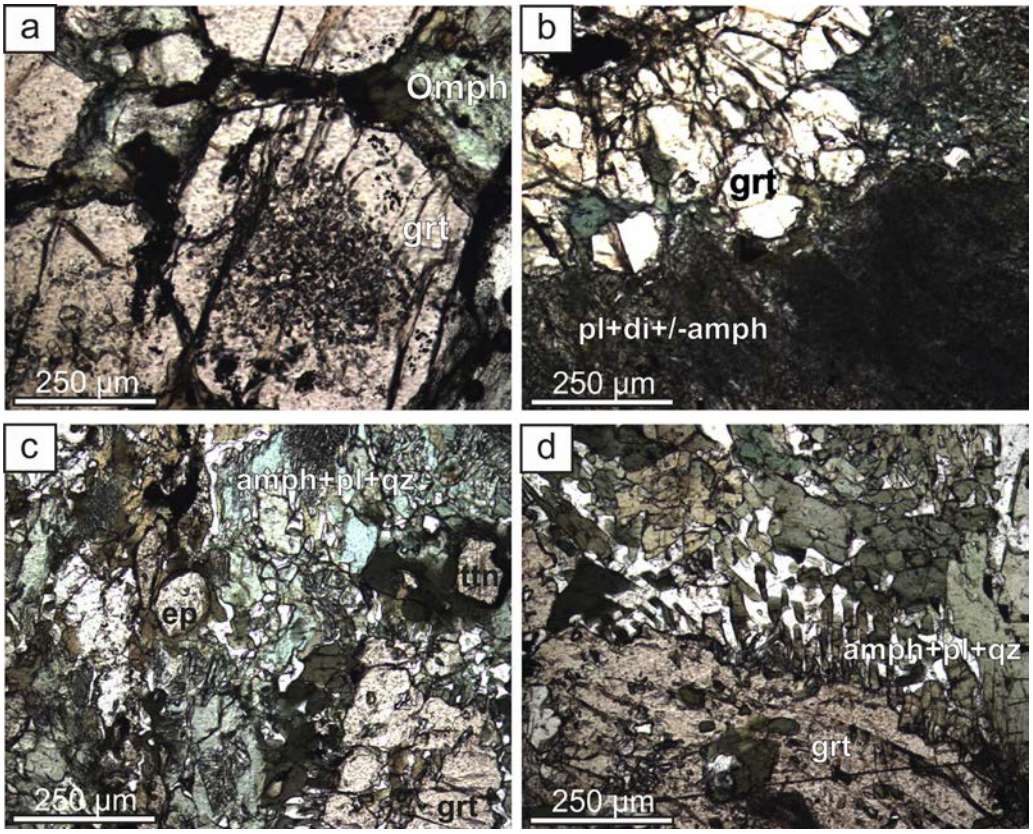

Fig. 3. Thin section images of preserved and retrogressed eclogites from the Tassendjanet. (a) Omphacite–garnet–rutile associations in sample Tinz 3. Note the numerous inclusions of omphacite (omph), quartz and rutile into garnet (grt). (b) Retrogressed eclogite showing plagioclase (pl)–diopside (di) symplectites after omphacite with limited blastesis of brown-green hornblende (amph) (Tinz 4). (c) Garnet-blue green and brown-green amphibole–epidote (ep)–titanite (ttn) assemblages in Til 6. Ilmenite is surrounded by titanite in the upper left corner of the image. (d) Brown-green amphibole, plagioclase, ilmenite and quartz intergrowths surrounding garnet in Til 6. (For interpretation of the references to colour in this figure legend, the reader is referred to the web version of the article.)

TINZ 3 sample considering a Fe_2O_3/FeO ratio (both values in wt%) of 0.1. It was constructed in the Na_2O-CaO-FeO-MgO-Al_2O_3-SiO_2-TiO_2-H_2O-Fe_2O_3 sub-system (NCFMASHTO) using the internally consistent dataset of Holland and Powell (1998, revised in 2003) and the free Gibbs energy minimization procedure with the software Perple_X (Connolly, 2005; Connolly, 2009). The solution models for heterogeneous phases are as follow: clino-amphibole (Diener et al., 2007), clinopyroxene (Green et al., 2007), garnet (White et al., 2007), feldspar (Holland and Powell, 2003), ilmenite (White et al., 2000). Except for retrograde phases, no hydrous minerals were observed in the eclogitic assemblage. The calculations made considering an anhydrous system failed to reproduce the measured minerals composition in TINZ 3, especially for garnet (see Inline Supplementary Fig. S1). In order to evaluate if water was present in the system at high pressure, a P–X_{H2O} diagram was drawn for a temperature fixed at 630 °C (Supplementary Fig. A). The modelled garnet compositions correspond to the measured values (XCa: 21, Mg#: 35) for a H_2O content around 0.3 wt% (=~1 mol% H_2O). This value was then used to compute a fixed-composition diagram for TINZ 3 (Fig. 6).

Inline Supplementary Fig. S1 can be found online at http://dx.doi.org/10.1016/j.precamres.2014.04.002.

The absence of plagioclase in the eclogite is consistent with high-pressure conditions above 12 kbar (Fig. 6). Quartz is present as some rare inclusions in garnet inner cores but it is absent in the matrix or in garnet rims, meaning that it can have formed during the prograde growth of garnet. Quartz is stable together with the observed eclogitic assemblage at low pressure 12–14 kbar and low temperature (<730 °C). The garnet isopleth corresponding to core composition (XCa: 21–22, Mg#: 35–36) cross at 600 °C, 13–14 kbar and also around 650 °C, 21 kbar (Fig. 6), in agreement with results of thermometry on omphacite–garnet pairs. The jadeite content measured in clinopyroxene is around 0.18–0.21 in the matrix but some inclusions are characterized by higher value, up to 0.24–0.26. The latter cannot be reproduced by the calculation but the modelled value at 650 °C, 21 kbar is between 0.19 and 0.20. According to the calculated isopleths, garnet inner rim composition, characterized by lower XCa (0.16–0.17) but higher XMg (0.37–0.38) compared to the cores, argues for lower *P–T* conditions, around 700 °C and 19 kbar. Outer rim compositions (XCa: 0.19–0.20, XMg: 0.38–0.40) defines two *P–T* ranges in the phase diagrams: 750 °C, 17 kbar and 650 °C, 12 kbar.

Another phase diagram was computed for the bulk composition of TINZ4 with a water content corresponding to 0.3 wt%. The eclogitic omphacite-bearing assemblage is not preserved in this sample but garnet shows different composition in the core and the rim. Garnet isopleths corresponding to core composition (XCa: 0.24–0.25, XMg: 0.33–0.34) do not exactly cross but converge in a narrow *P–T* domain around 640 °C, 22 kbar (Fig. 7), in agreement with the results from TINZ 3.

4.2. Retrograde path

According to phase diagrams built for water undersaturated conditions (Figs. 6 and 7), the retrogression of omphacite and garnet into plagioclase bearing assemblages occurred below 14 kbar. The low jadeite content in clinopyroxene of sample TINZ 4 (0.10–0.20) is compatible with low pressure of equilibration, below 14 kbar.

A water-saturated system was considered for the retrogressive stage as most prograde phases are partly or totally transformed

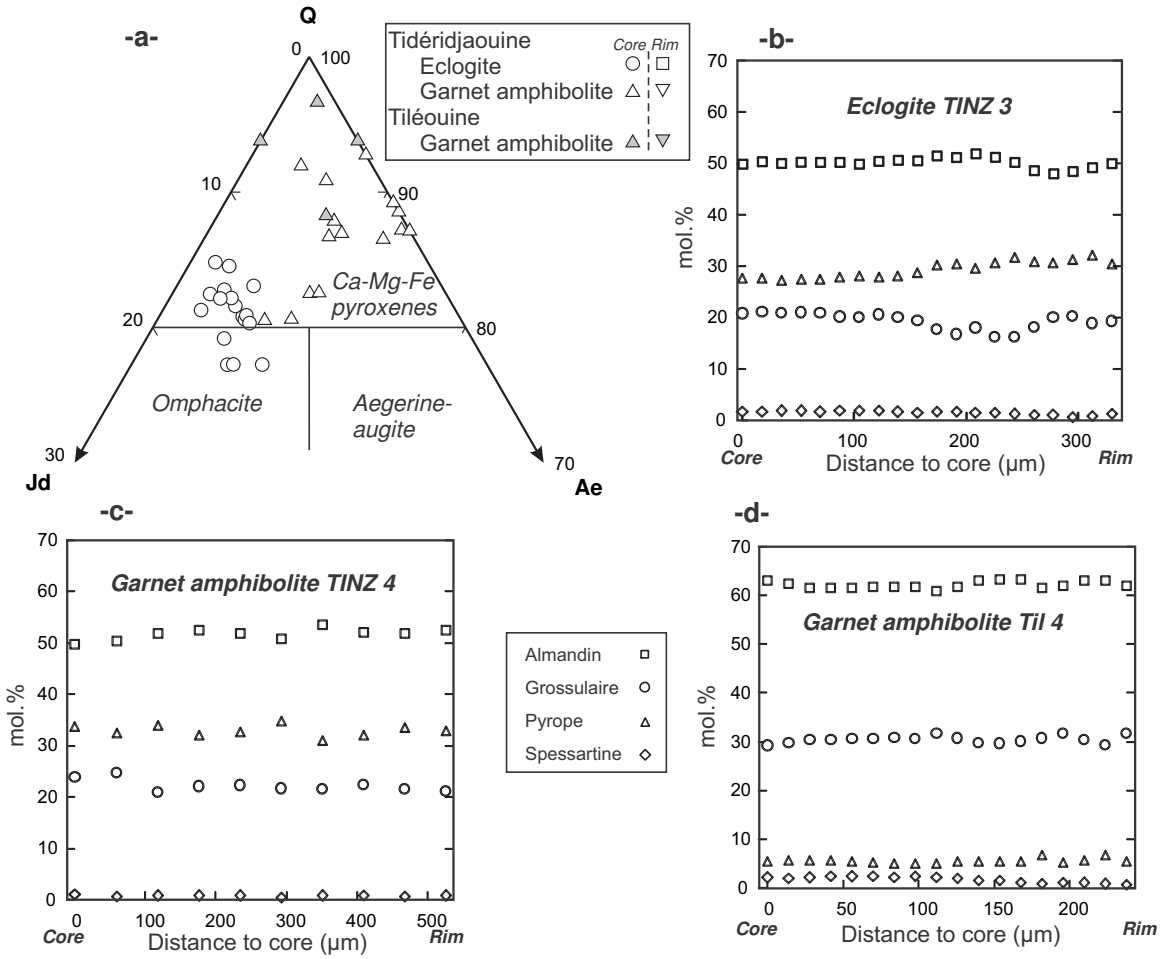

Fig. 4. Composition of garnet and clinopyroxene in eclogite and amphibolites from the Tassendjanet terrane. (a) Pyroxenes plotted in the Aegerine-Jadeite-quadrilateral components diagram. (b–d) Core to rim microprobe traverse in garnet from eclogite Tinz 3 and garnet amphibolites Tinz 4 and Til 4.

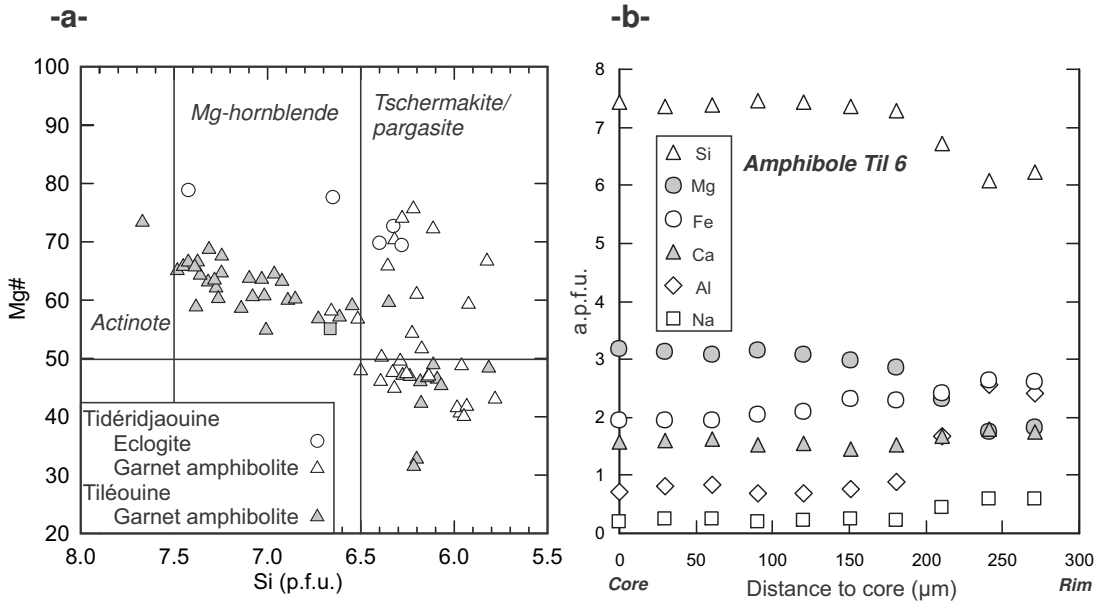

Fig. 5. Composition of amphiboles from retrogressed Tassendjanet eclogites. (a) Classification diagram of Leake et al. (1997). (b) Zoning profile in a brown-green hornblende with a blue-green tschermakitic rim (Til 6).

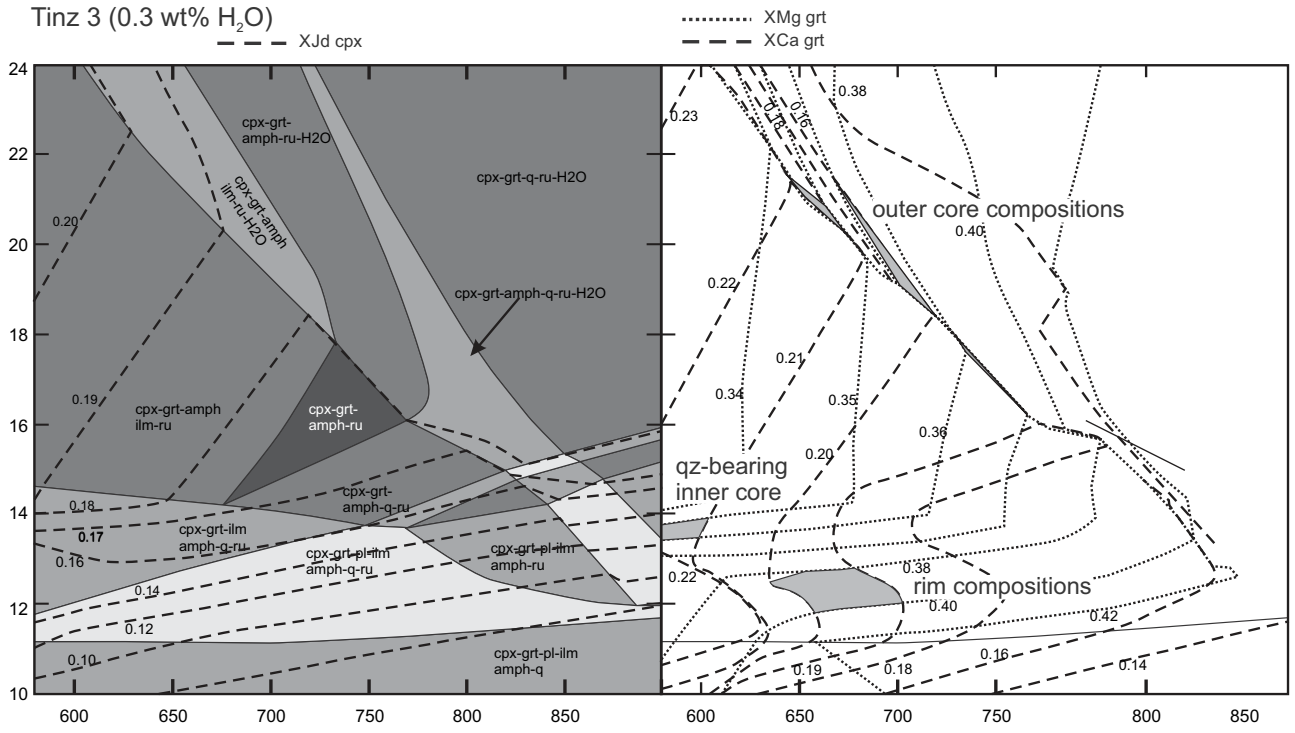

Fig. 6. Fixed-composition phase diagram built for the bulk composition of TINZ 3 + 0.3 wt% H_2O. Isopleth of Jd content in clinopyroxene and XMg and XCa in garnet are also represented.

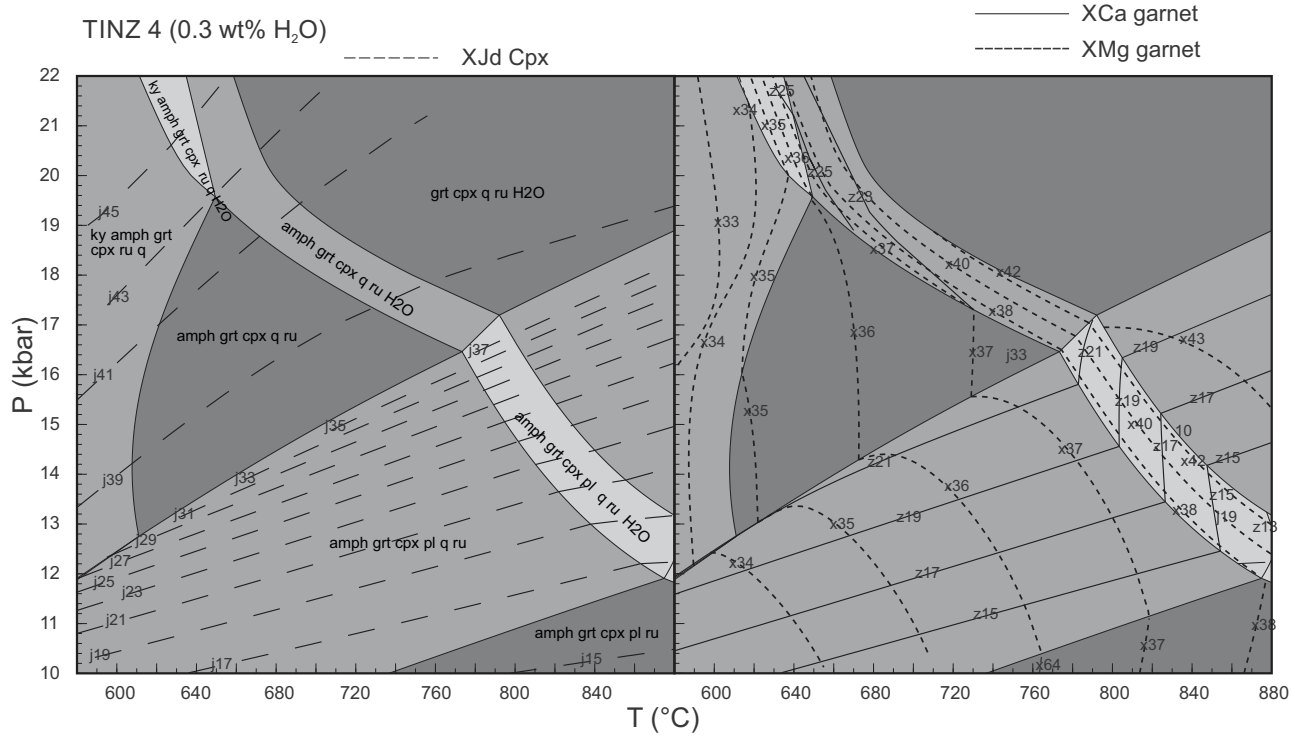

Fig. 7. Fixed-composition phase diagram built using the bulk composition of TINZ 4 + 0.3 wt% H_2O. Isopleth for Jd content in clinopyroxene and XMg and XCa in garnet are also represented.

into hydrous assemblages. A fixed-composition phase diagram has been built for the garnet amphibolite TINZ 4 (Fig. 8), still showing plagioclase–diopside intergrowth after omphacite but characterized by the blastesis of green amphibole around garnet and in the textural site of plagioclase–diopside intergrowths.

The assemblage garnet–plagioclase–amphibole–diopside–quartz–titanite–ilmenite observed in the retrogressed eclogites is stable at *P–T* conditions around 680 °C and 10 kbar. Modelled garnet composition however failed to reproduce those measured in the rim. During retrogression, rutile progressively transformed

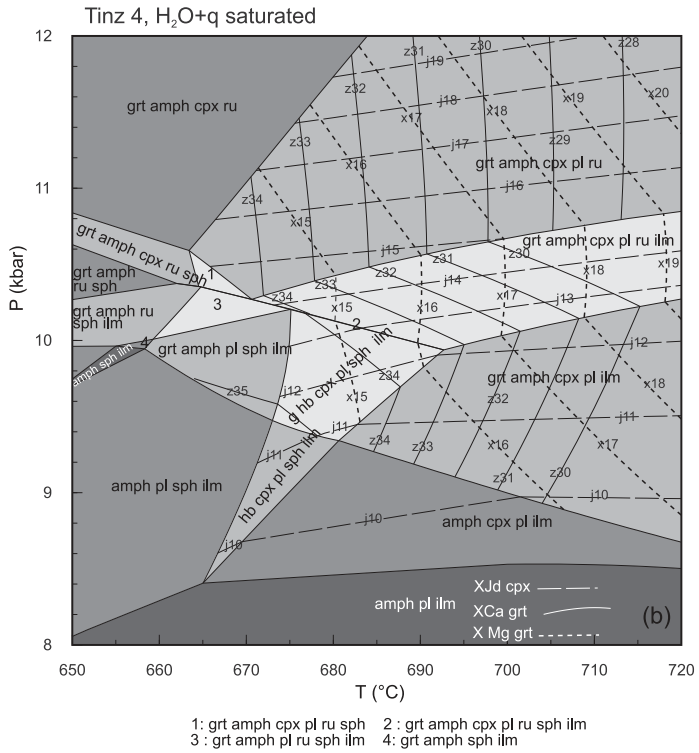

Fig. 8. Fixed-composition phase diagram built using the water-saturated bulk composition of TINZ 4.

to ilmenite which is in turn surrounded by titanite (Fig. 3c). Following the topology of the phase diagram, the transition from rutile to titanite occurred between 680 and 700 °C at 9–11 kbar in sample TINZ 4 (Fig. 8) and around 14 kbar for sample TINZ 3 (Fig. 6).

The hornblende–plagioclase thermometer of Holland and Blundy (1994) and the garnet–amphibole–plagioclase–quartz (GASP) barometer of Kohn and Spear (1990) were applied on hornblende–plagioclase coronas surrounding garnet. Calculated *P–T* conditions cover a large range, between 7 and 10 kbar for temperatures comprised between 610 °C and 740 °C (see Fig. 15), consistently with results deduced with isochemical phase diagrams. No systematic differences between samples from Tiléouine and Tidéridjaouine were observed concerning the retrograde path.

4.3. Major and trace-element geochemistry

The three samples from Tiléouine have globally similar compositions (Fig. 9, Table 2) characterized by 47–49% SiO_2, high Ti (3 wt% TiO_2) and Fe content (FeOt: 15–16 wt%) but low Al and alkalis (12–13 and 2–3 wt%, respectively). The major element composition is strikingly similar to continental tholeiites from the Central Atlantic magmatic province and especially those from Guyana (Deckart et al., 2005).

Samples from Tidéridjaouine have much more scattered compositions (Fig. 9, Table 2). TINZ 1 and TINZ 4 are comparable to Tiléouine samples in terms of major elements except for slightly higher Mg and Ca contents but lower Ti and Fe. TINZ 5 shows lower Si and Ti (45 and 1.7 oxide wt%, respectively) contents but higher Al and Ca values (15 and 14 oxide wt%), which can indicate segregation of plagioclase in the igneous precursor. Sample TINZ 3 has a distinct composition from all other samples, it has the lowest SiO_2, Al_2O_3 and Na_2O contents (44, 11.5 and 1.3 wt%, respectively) with high TiO_2 (4.8 wt%) and MgO values (10.3 wt%).

In the TAS and AFM diagrams (Fig. 9), all samples plot in the subalkaline and tholeiitic field. Because alkalis can be readily mobile during metamorphism (see Section 8.2), the studied rocks have also been plotted in the Winchester and Floyd (1977) diagram for a classification using immobile trace-elements only (Fig. 9). All garnet amphibolites fall in the subalkaline basalts field, except the eclogite TINZ 3 which has the trace element characteristics of alkaline basalts. The FeO/MgO vs SiO_2 diagram of Miyashiro (1974) confirms that the studied subalkaline metabasalts are of tholeiitic affinity (Fig. 9). The low Sr contents of most samples (130–229 ppm) and the low Cr values (61–328 ppm) argue that the eclogites are former basaltic melts rather than cumulates. This is confirmed by the absence of positive Eu anomalies (Eu/Eu*: 0.9–1.0) in REE patterns (Fig. 10a). By contrast, TINZ 5 is characterized by a slight positive Eu anomaly (Eu/Eu*: 1.1), the highest CaO and Al_2O_3 values (14.6 and 15.5 wt%, respectively) and high Sr contents (1640 ppm) which is a fingerprint of plagioclase cumulates (Fig. 10).

The three samples from Tiléouine have similar E-MORB like trace-element patterns (Fig. 10). They show enrichment in LREE ($(La/Sm)_N$: 1.28–1.31), slight negative Eu anomalies and normalized REE contents between 10 and 100 times the chondrites (Fig. 10a). N-MORB normalized multi-elements patterns show a relative enrichment of the most incompatible elements (U, Th, Nb, Ta) relative to Zr, Hf and HREE with a positive spike in Pb (Fig. 10b). TIL 6 has no negative anomaly in K and Rb but samples TIL 4 and TIL 9 show pronounced depletion in these two elements (K/K*: 0.68 and 0.38, respectively). The amplitude of this negative anomaly is moreover negatively correlated with Ba and Pb contents for the three samples from Tiléouine (Fig. 11).

The Tidéridjaouine samples have much more variable trace-elements compositions. REE pattern of TINZ 5 and TINZ 1 (Fig. 10a) are comparable to those of Tiléouine amphibolites except for a slight positive Eu anomaly for TINZ 5 and a steeper LREE slope ($(La/Sm)_N$: 2.11) for TINZ 1. They also show enrichment in the most incompatible elements (Ba, Th, U) compared to Tiléouine samples (Fig. 10b) and TINZ 5 shows a slight depletion in Zr, Hf and Ti. TINZ 3 is strongly enriched in most trace-element compared to other samples (Zr: 397 ppm; Nb: 45 ppm; Th: 11 ppm), it

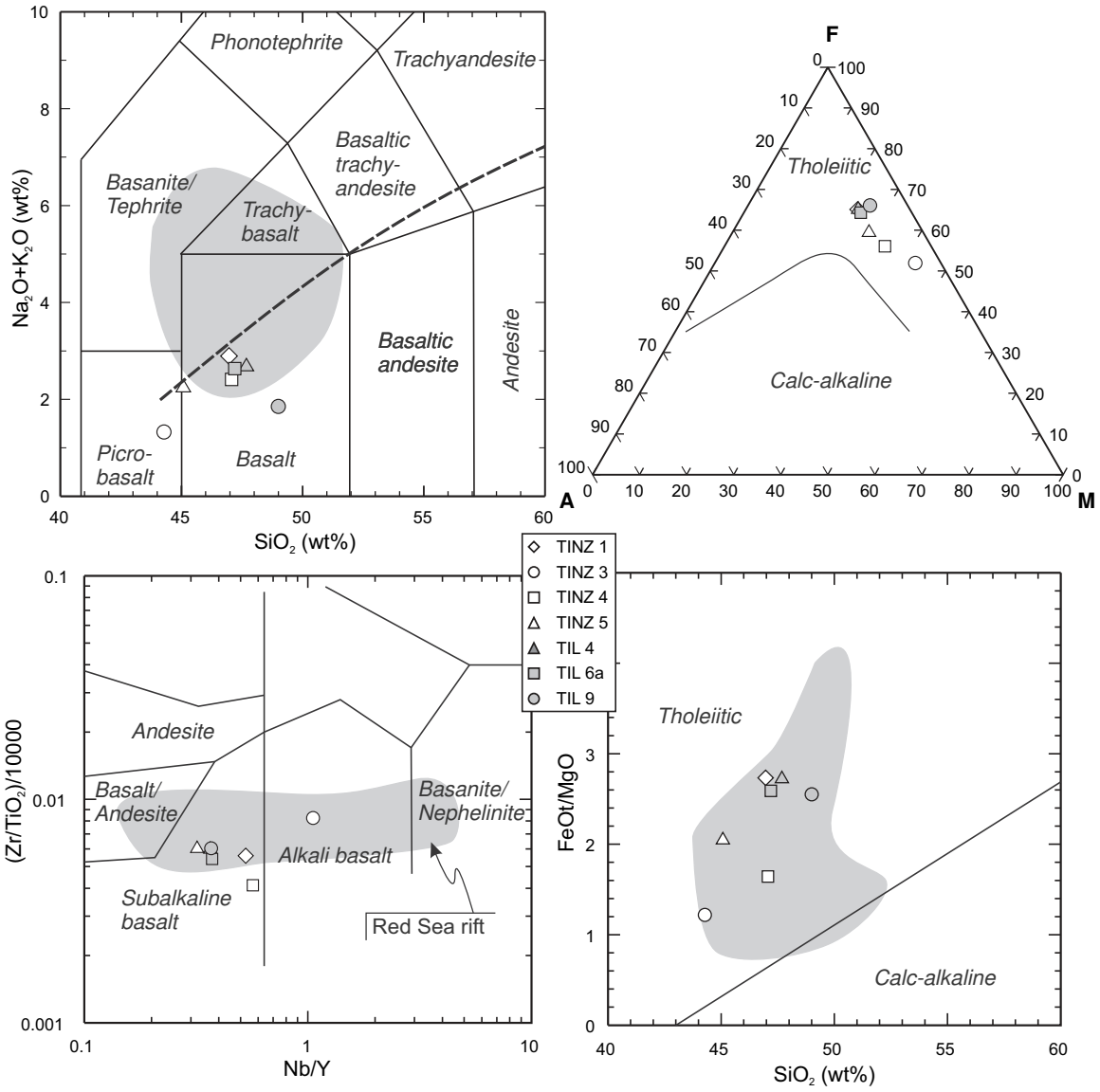

Fig. 9. Classification of Tiléouine-Tidéridjaouine eclogite and amphibolites in various diagram for igneous rock classification.

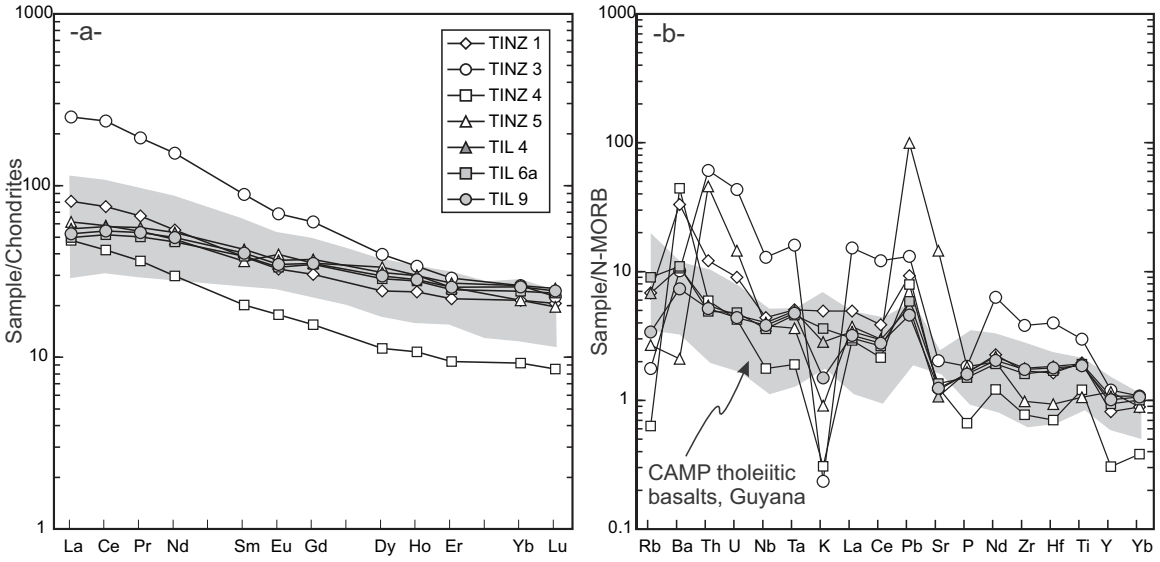

Fig. 10. REE (a) and multi-element patterns (b) of Tassendjanet eclogites and amphibolites. The CAMP basalts are from Deckart et al. (2005). Normalization values from McDonough and Sun (1995) and Hofmann (1988).

Table 2
Major and trace-elements composition of the Tassendjanet eclogite and garnet amphibolites.

	TINZ 1	TINZ 3	TINZ 4	TINZ 5	TIL 4	TIL 6	TIL 9
Major elements (wt%)							
SiO_2	46.96	44.28	47.07	45.08	47.68	47.20	49.00
TiO_2	3.15	4.83	1.95	1.70	3.10	3.09	2.99
Al_2O_3	12.77	11.50	14.87	15.52	12.60	12.28	12.09
FeOt	18.82	13.94	15.27	12.79	17.57	17.31	16.98
MnO	0.22	0.22	0.14	0.15	0.25	0.23	0.23
MgO	6.19	10.29	8.36	5.63	5.81	6.01	5.99
CaO	8.75	12.36	10.18	14.58	9.30	9.82	9.52
Na_2O	2.37	1.30	2.38	2.14	2.37	2.25	1.69
K_2O	0.52	0.03	0.03	0.10	0.30	0.38	0.16
P_2O_5	0.31	0.34	0.12	0.34	0.31	0.28	0.30
LOI	0.18	−0.37	−0.24	0.85	−0.50	−0.37	−0.36
Sum	100.25	98.71	100.15	98.87	98.80	98.50	98.58
Trace-elements (ppm)							
Co	107	84	78	47	72	71	72
Cr	61	215	328	168	173	180	195
Cu	135	120	355	10	357	292	304
Ni	57	153	148	71	60	62	61
Sc	49	29	42	26	43	43	43
V	545	369	512	382	409	414	397
Zn	166	67	102	85	145	152	145
Rb	8.6	2.2	0.8	3.4	8.6	11.4	4.3
Sr	135	230	142	1637	121	153	141
Y	29.2	42.9	10.9	41.6	38.5	33.7	36.2
Zr	176	398	81	102	185	167	181
Nb	15.4	45.2	6.2	13.3	14.1	12.6	13.4
Ba	460	141	616	29	149	152	101
La	19.2	59.5	11.4	14.6	13.3	11.8	12.4
Ce	46.3	145.6	25.8	35.9	35.3	31.6	33.3
Pr	6.18	17.6	3.37	5.03	5.28	4.66	4.93
Nd	25.2	70.7	13.6	22.2	24.3	21.5	22.8
Eu	1.84	3.86	1.00	2.23	2.07	1.88	1.95
Sm	5.70	13.2	2.98	5.37	6.29	5.74	5.97
Gd	6.04	12.2	3.08	7.03	7.40	6.93	7.02
Dy	5.98	9.77	2.77	8.24	7.66	7.05	7.33
Ho	1.31	1.85	0.59	1.64	1.63	1.52	1.55
Er	3.51	4.63	1.51	4.08	4.32	3.96	4.10
Yb	3.45	4.21	1.49	3.46	4.20	3.91	4.14
Lu	0.51	0.56	0.21	0.48	0.62	0.58	0.60
Hf	4.85	11.84	2.09	2.77	5.45	5.04	5.30
Ta	0.97	3.08	0.36	0.70	0.95	0.88	0.91
Pb	4.52	6.42	3.87	48.7	2.59	2.87	2.24
Th	2.27	11.4	1.11	8.56	1.02	0.92	0.96
U	0.64	3.07	0.30	1.03	0.33	0.34	0.31

shows a steep REE pattern ($(La/Yb)_N$: 9.59) with high LREE contents (La: 59 ppm)(Fig. 10) typical of alkali basalts. Pronounced negative spikes are observed for Rb, K, Pb and Sr. By contrast, TINZ 4 is depleted in most trace element when compared to other samples, it also shows a LREE enriched pattern ($(La/Sm)_N$: 2.39) but with low REE values, and is characterized by deep negative anomalies for Rb and K (Figs. 10 and 11).

4.4. Zircon U–Pb geochronology

The fresh eclogite TINZ 3 displays small minute anhedral to subhedral zircons (less than 40 μm width) in the omphacite-dominated matrix and sometimes as inclusions into the rim of garnet. Grains are most of the time in direct contact with rutile and ilmenite; these minerals can indeed have been the main provider of Zr during metamorphism (Bingen et al., 2001; Dhuime et al., 2007). Zircon is also always found in textural microdomains where retrograde amphibole or ilmenite developed. Backscattered electron images of the zircons did not show any compositional zoning, or mineral inclusions (Fig. 11).

Even if zircon is relatively abundant in thin section, not enough material was available to separate zircon from its host rock and to mount it together with a standard, especially when considering its small size comprised between 15 and 30 μm. U–Pb age was thus acquired on the thin section itself. The diameter of the laser beam was set at down to 15 μm to prevent ablation of surrounding phases during acquisition. Because of the small size of the zircons, the laser beam frequently passed through the grains. Therefore, only the part of ablation spectra corresponding to zircon was selected for dating and for calculation of the U, Pb and Th concentrations. Results are presented in Table 3 and Fig. 12. Dating zircons directly in thin sections allow to have a petrographic control on its textural position relatively to preserved eclogitic assemblages or retrograde domains (Gao et al., 2011; Zhou et al., 2011). Unfortunately, due to the small size and limited number of zircon grains in TINZ 3, it was not possible to perform trace-element analyses of zircons, as all grains were destroyed during U–Pb LA–ICP–MS analysis.

Amongst the 16 valid spots (i.e., those ablating zircon during at least 15–20 s), one is strongly discordant while the remaining are concordant or slightly discordant (<10% discordance). If the 15 concordant to slightly discordant spots are used for calculation, the discordia age is 623 ± 7 Ma (Fig. 12) with a meaningless upper intercept (6 ± 9 Ga). Most zircons have very low Th/U ratios below 0.1, with 10 spots <0.05, and only two grains display higher ratios of 0.32 and 0.36 (Table 3). When the two last analyses are excluded together with the largely discordant spot and one showing very large errors on the measured ratios, the discordia age is 622 ± 7 Ma (Fig. 12). The concordant age obtained by excluding

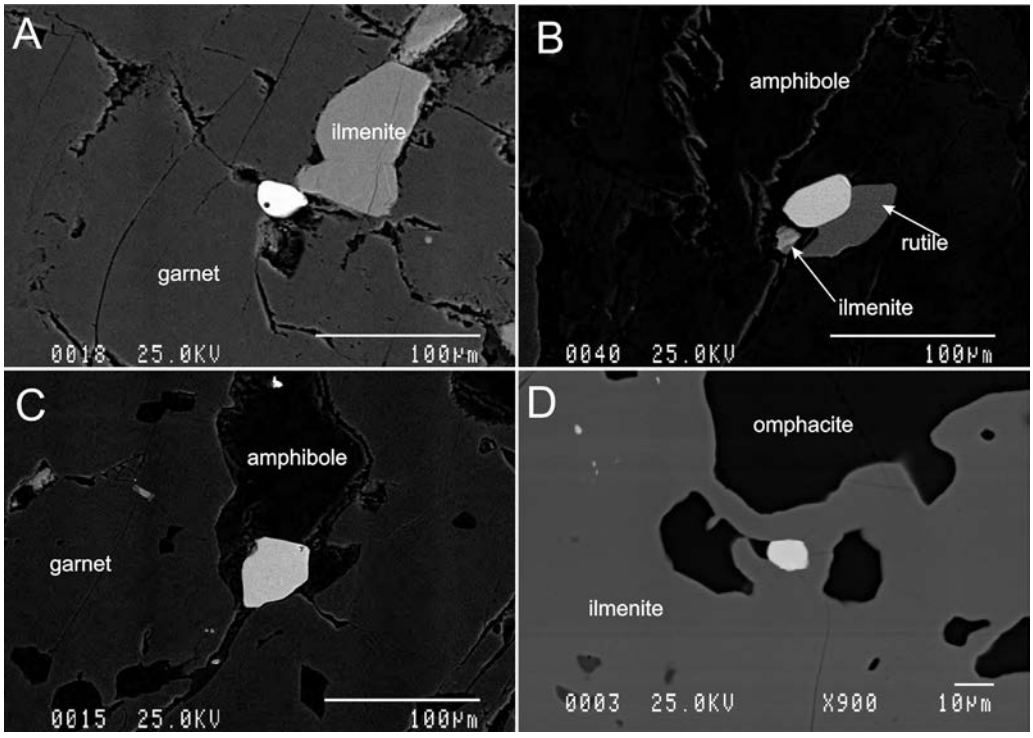

Fig. 11. Backscattered electron images of zircon in eclogite TINZ 3. (A) zircon bordering ilmenite included into garnet. (B) Rutile–ilmenite–zircon association in a retrograde amphibole-bearing domain. (C) Zircon associated to amphibole included in garnet. (D) Tiny zircon included in a retrograde ilmenite.

slightly to largely discordant zircons (8 grains remaining with less than 2% discordance) is 623 ± 2 Ma (Fig. 12). The weighted average of $^{206}Pb/^{238}U$ ages on 15 concordant to slightly discordant spots (the largely discordant is excluded) is 622 ± 5 Ma.

4.5. Sr–Nd isotopic composition

The magmatic emplacement age of the eclogite and amphibolites precursors is not known. Consequently, the initial isotopic compositions cannot be calculated precisely, only the values that prevailed during the metamorphism can be. However, according to U–Pb zircon dating (see discussion), the precursor of the eclogites has been emplaced before 623 Ma. On the seven values, five eclogite and amphibolite Nd T_{DM} model ages (calculated using the depleted mantle evolution model of Nelson and DePaolo, 1984) range between 0.8 Ga and 1.3 Ga, the two additional values being at 1.9–2 Ga (Table 4). This indicates that the studied eclogites and amphibolites resulted from the mixing of a <0.8 Ga juvenile mantle source and a Paleoproterozoic or Archean crustal source, in variable amount. The protolith of these rocks emplaced between 623 and 800 Ma. Following Caby and Monié (2003), pulses of mafic magmatism have been evidenced at around 800 Ma (tholeiitic mafic sills) and just before 680 Ma (Ar–Ar age on a late magmatic pargasite from the Ougda complex). For the calculation of Sr and Nd isotopic initial ratios, a crystallization age for the magmatic precursor was arbitrarily fixed at 700 Ma. If the igneous age is considered 100 Myr younger or older, it will only induce a shift ranging between ±0.00001 and ±0.0003 for the $^{87}Sr/^{86}Sr$ ratio (due to very low Rb/Sr ratios) and less than 1 unit for ε_{Nd} values.

The three samples from Tiléouine are in a narrow range of isotopic composition comprised between +4 and +6 for ε_{Nd} and 0.7056 and 0.7076 for $(^{87}Sr/^{86}Sr)_i$ Table 4, Fig. 13). These compositions are slightly more radiogenic than the depleted MORB mantle (DMM) at 700 Ma which is at +7.5 (calculated using the data from Workman and Hart (2005) considering a single stage linear evolution). Tidéridjaouine samples have more radiogenic composition, ε_{Nd} down to −6 and $(^{87}Sr/^{86}Sr)_i$ up to 0.7173 (Table 4, Fig. 13).

As there is no geochemical or isotopic data on the basement rocks from the Tassendjanet terrane, a quantitative estimation of crustal contamination in the mantle source (source contamination) of the igneous precursors or during magma emplacement (crustal assimilation) cannot be performed. Two qualitative mixing models were computed on the Sr–Nd plot (Fig. 13) using data from the Depleted MORB Mantle (DMM) and mean Upper Continental Crust (UCC). For the UCC component, the mean of the Archean/Paleoproterozoic rocks from In Ouzzal was selected for age-corrected isotopic ratios while Sr and Nd concentrations were those of mean upper crust (Rudnick and Gao, 2003). Sr–Nd concentrations and isotopic ratios (recalculated at 700 Ma) for DMM are those from Workman and Hart (2005). The first mixing curve represents the mélange between DMM and the old radiogenic upper UCC and can be interpreted as source contamination. The second one represents crustal assimilation where the end-members are the retrogressed eclogite with the highest ε_{Nd} (less contaminated basaltic precursor) and the same UCC component. Source contamination requires mixing of less than 2 wt% of UCC component in a depleted mantle to obtain the isotopic composition of the igneous precursors. In the case of crustal assimilation, more than 30 wt% of crustal material has to be mixed with mantle-derived basalt to reproduce the most radiogenic signature of the most radiogenic retrogressed eclogite (TINZ 4).

5. Discussion

5.1. Pressure-temperature evolution of the eclogite and garnet amphibolites

Results from isochemical phase diagrams (for TINZ 3 and 4) and garnet-omphacite thermometry both converge to conditions around 630 °C and 21 kbar for the eclogitic stage. Garnet cores

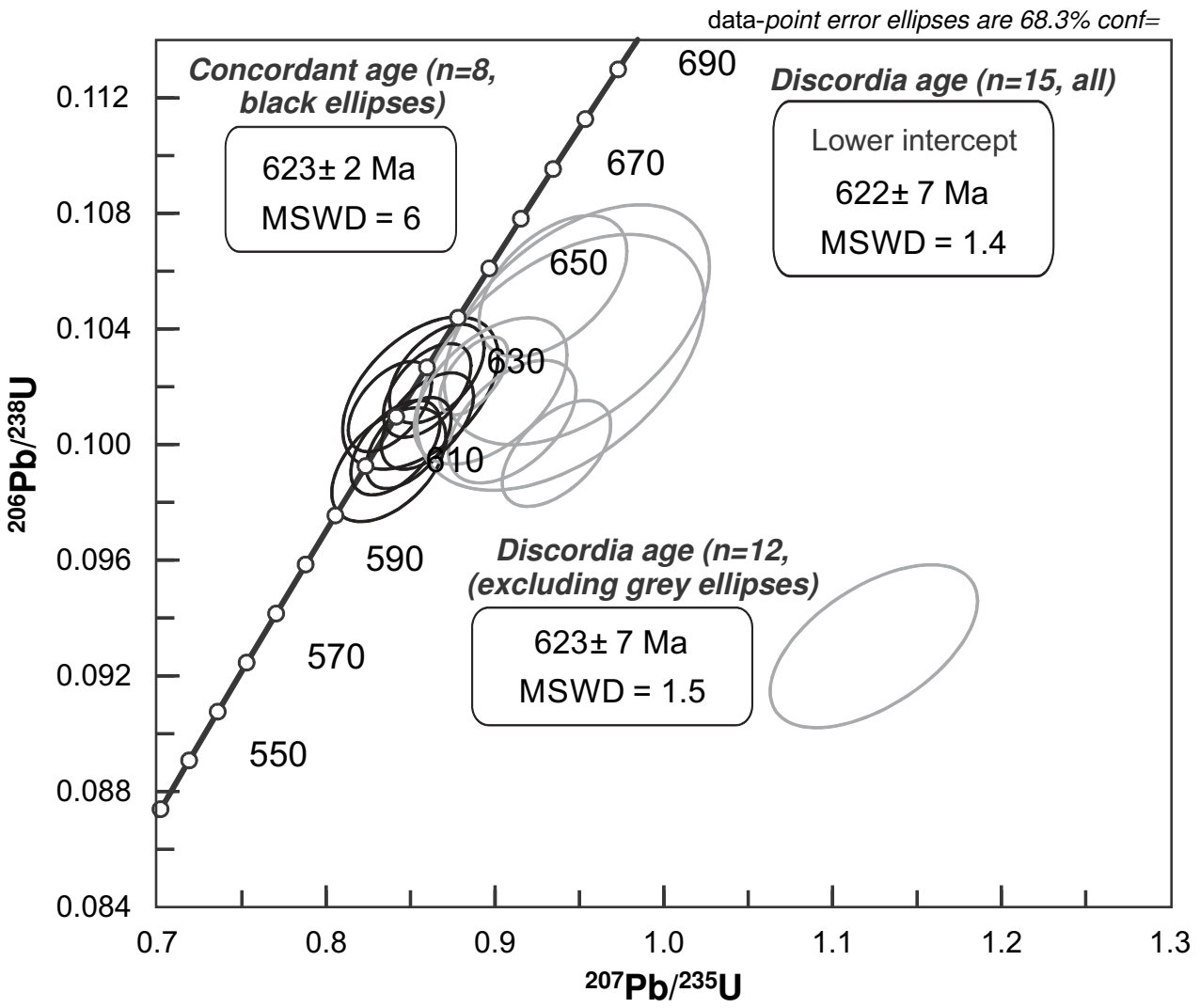

Fig. 12. Concordia plot for the metamorphic zircons in the eclogite TINZ 3.

containing few quartz inclusions could have kept the memory of earliest prograde path (Fig. 14): a PT increase from 580 °C, 13–14 kbar (where quartz is stable) to the peak conditions cited above (where quartz is not stable) would not have modified the composition of garnet as XMg and XCa isopleth are nearly parallel to the path (Fig. 6). Additionally, omphacite inclusions into garnet are richer in jadeite content compared to the matrix. This is probably a consequence of fractional crystallization or open system behaviour during prograde metamorphism; such high jadeite contents cannot be reproduced with thermodynamic models for the measured bulk composition of TINZ 3. Garnet in TINZ 3 preserved zoning characterized by a decrease in grossular content towards the inner rim, than by an increase to 20 mol% in the outer rim while the Mg# gently increase from core to rim. This chemical zoning is related to a decrease of pressure and a slight increase in temperature to 730 °C, 18 kbar (Fig. 14). The development of amphibole–plagioclase rims around garnet has been constrained to 610–740 °C at 7–10 kbar (Fig. 14) with empirical thermobarometers. The same conditions are obtained from phase transitions from rutile to ilmenite and from ilmenite to titanite (Fig. 8). Heating starting after peak pressure is probably a consequence of continental crust stacking and thermal relaxation when subduction ends. Cold subducted continental crust has two source of heat: conductive heating from surrounding hotter mantle and radioactive decay in the subducted upper crust (Clark et al., 2011). Post-pressure peak heating during exhumation is typical of the metamorphic path of continental eclogites involved in collisional orogens, for example in the Dabie Shan orogen (Carswell and Zhang, 1999; Zhao et al., 2007; Gao et al., 2011). It can eventually lead to high-pressure partial melting of the felsic and metasedimentary rocks surrounding eclogites or fluid expulsion from hydrous HP rocks (Labrousse et al., 2002; Xia et al., 2008). These authors invoke thermal relaxation (linked to the global relatively low speed of the exhumation process during collisions) or lithospheric delamination to explain heating of the cold subducted continental slab after peak pressures have been reached. The last step of *P–T* evolution registered by the samples is marked by the association of epidote and blue-green amphibole around the rim of garnet. It is an evidence for partial reequilibration in the epidote-amphibolite facies at temperature between 500 and 650 °C for pressures around 4–8 kbar (Fig. 14).

5.2. Causes of mobile elements depletion

Most samples are characterized by deep negative K and Rb anomalies in mutli-element plots (Fig. 10b) with low Na contents, whereas rift basalts with the same immobile trace-elements distribution show no negative K or Rb anomaly and higher Na contents (Figs. 9 and 10). TINZ 3 has the trace-element fingerprint of an

Table 3
Results of zircon U–Pb dating for sample TINZ 3.

Analysis_#	Pb ppm	Th ppm	U ppm	Th/U	$^{207}Pb/^{235}U$ Value	$^{207}Pb/^{235}U$ ± abs (1σ)	$^{206}Pb/^{238}U$ Value	$^{206}Pb/^{238}U$ ± abs (1σ)	$^{207}Pb/^{206}Pb$ Value	$^{207}Pb/^{206}Pb$ ± abs (1σ)	Age $^{207}Pb/^{235}U$	± abs (1σ)	Age $^{206}Pb/^{238}U$	± abs (1σ)	Disc. (%)
aa_2	32.3	3.1	377	0.01	0.856	0.030	0.1018	0.0017	0.0610	0.0024	625	10	628	16	0.5
aa_3	29.7	4.6	337	0.01	0.934	0.029	0.1055	0.0016	0.0642	0.0022	646	9	670	15	3.6
aa_4	10.0	9.6	90	0.11	1.124	0.041	0.0930	0.0019	0.0878	0.0035	573	11	765	19	33.4
aa_7	51.4	4.9	592	0.01	0.866	0.019	0.1025	0.0011	0.0613	0.0015	629	7	633	10	0.7
aa_8	71.9	8.1	851	0.01	0.838	0.016	0.1013	0.0010	0.0600	0.0013	622	6	618	9	0.7
aa_9	33.0	16.7	391	0.04	0.949	0.052	0.1041	0.0027	0.0661	0.0039	639	16	677	27	6.1
aa_10	60.7	32.2	728	0.04	0.910	0.025	0.1008	0.0014	0.0655	0.0020	619	8	657	13	6.2
ab_10	21.3	18.0	219	0.08	0.936	0.021	0.0997	0.0012	0.0681	0.0017	613	7	671	11	9.5
ab_1	76.7	34.6	861	0.04	0.888	0.013	0.1024	0.0009	0.0629	0.0011	628	5	645	7	2.7
ab_2	44.4	5.9	509	0.01	0.860	0.017	0.1019	0.0011	0.0612	0.0014	625	6	630	9	0.8
ab_3	33.4	6.7	390	0.02	0.860	0.018	0.1008	0.0011	0.0619	0.0015	619	6	630	10	1.8
ab_4	48.3	8.2	586	0.01	0.841	0.017	0.0999	0.0011	0.0611	0.0014	614	6	620	10	1.0
ab_7	10.4	40.0	125	0.32	0.837	0.022	0.0993	0.0013	0.0612	0.0018	610	8	618	12	1.2
ab_8	21.3	18.0	219	0.08	0.849	0.017	0.1001	0.0010	0.0616	0.0014	615	6	624	9	1.5
ab_9	16.0	31.4	87	0.36	0.939	0.056	0.1028	0.0029	0.0663	0.0043	631	17	672	29	6.5
ab_14	29.8	20.3	357	0.06	0.897	0.030	0.1019	0.0017	0.0639	0.0023	625	10	650	16	4.0

Table 4
Sr–Nd isotopic composition of Tileouine-Tideridjaouine samples.

Sample	Sr	Rb	$^{87}Rb/^{86}Sr$	2 σ	$^{87}Sr/^{86}Sr$	2 σ	$^{87}Sr/^{86}Sr$ 623 Ma	$^{87}Sr/^{86}Sr$ 700 Ma	$^{87}Sr/^{86}Sr$ 800 Ma	$^{87}Sr/^{86}Sr$ 2000 Ma	Sm	Nd	$^{147}Sm/^{144}Nd$	2 σ	$^{143}Nd/^{144}Nd$	2 σ	ε_{Nd} 623 Ma	ε_{Nd} 700 Ma	ε_{Nd} 800 Ma	ε_{Nd} 2000 Ma	TDM (Ma)
TIL4	121	8.6	0.205	0.012	0.708465	0.000009	0.70664	0.70642	0.70612	0.70256	6.3	24.3	0.1564	0.0031	0.512749	0.000007	5.4	5.8	6.3	12.6	797
Til6	153	11.4	0.215	0.012	0.709805	0.000010	0.70789	0.70765	0.70734	0.70360	5.7	21.5	0.1616	0.0032	0.512698	0.000013	4.0	4.3	4.8	10.2	1014
TIL9	141	4.3	0.088	0.005	0.706473	0.000007	0.70569	0.70559	0.70547	0.70393	6.0	22.8	0.1584	0.0032	0.512712	0.000009	4.5	4.9	5.4	11.3	921
TINZ1	135	8.6	0.184	0.011	0.713074	0.000009	0.71144	0.71123	0.71097	0.70776	5.7	25.2	0.1369	0.0027	0.512045	0.000007	−6.8	−6.2	−5.5	3.8	1978
TINZ3	230	2.2	0.028	0.002	0.715285	0.000007	0.71504	0.71500	0.71496	0.71447	13.2	70.7	0.1127	0.0023	0.512186	0.000011	−2.1	−1.3	−0.2	12.8	1291
TINZ4	142	0.8	0.016	0.001	0.717448	0.000010	0.71730	0.71729	0.71726	0.71698	3.0	13.6	0.1326	0.0027	0.512015	0.000009	−7.1	−6.4	−5.6	4.3	1929
TINZ5	1637	3.4	0.006	0.001	0.711468	0.000007	0.71142	0.71141	0.71140	0.71130	5.4	22.2	0.1465	0.0029	0.512478	0.000011	0.9	1.4	2.0	9.8	1277

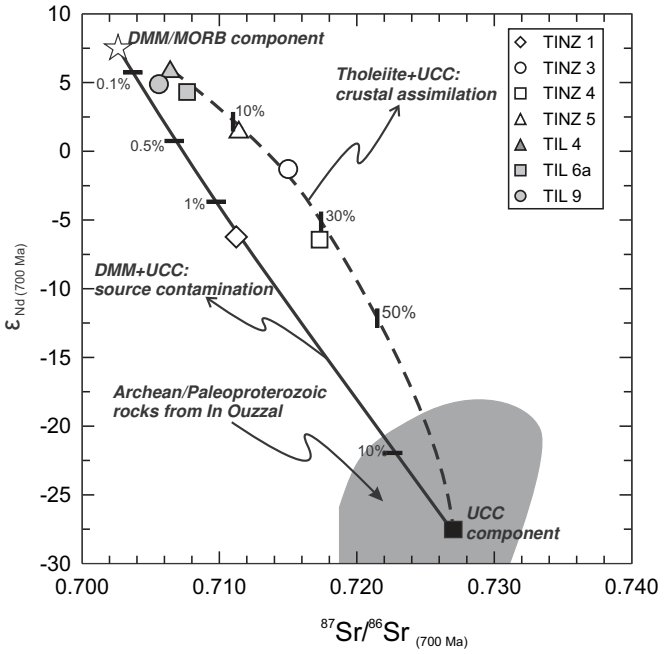

Fig. 13. Initial Sr and Nd composition of the investigated samples. The composition of the depleted mantle has been calculated with the data of Workman and Hart (2005) considering a linear, one-stage evolution. The field of Archean/Paleoproterozoic gneisses is from Ait-Djafer et al. (2003). The percentages represent the weight fraction of contaminant. See text for detailed explanation on mixing curves.

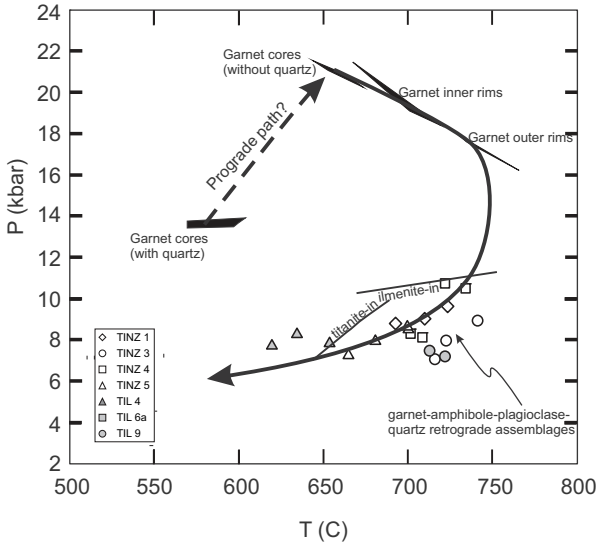

Fig. 14. Summary of *P–T* conditions estimated for the Tiléouine-Tidéridjaouine eclogite and amphibolites and proposed *P–T* path. Points are the results of GASP and hornblende–plagioclase thermobarometry for the retrograde stage.

alkali basalt but it has low alkali contents (Na_2O: 1.2 wt% and K_2O: 0.03 wt%). For samples of the Tiléouine area, the amplitude of the negative K anomaly is correlated with a decrease in Rb, Ba and Pb contents but also with a decrease of $^{87}Sr/^{86}Sr$ ratios calculated at 623 Ma. Considering that these anomalies only affect mobile elements, we can conclude that they originated by fluid-rock interactions. The eclogite TINZ 3 is almost not retrogressed but displays the deepest depletion in alkalies. Thin amphibole–plagioclase rims develop around garnet but omphacitic pyroxene (the only primary sodium carrier in this rock) is well preserved, so the leaching of alkalies did not occur during retrogression.

The jadeite content of TINZ 3 clinopyroxene is low, between 18 and 26 mol% (Fig. 4). If an alkaline basalt is metamorphosed to the same conditions, the jadeite content of pyroxene would have been around 40–45 mol% (according to fixed-composition phase diagram for an unleached alkaline basalt from the Dead Sea (Alici et al., 2001) with similar Ca, Mg, Al and Si contents, not shown). We can thus place the main fluid-rock interaction event before the growth of omphacitic pyroxene. Considering the three samples from Tiléouine, the one showing no negative anomaly for K and normal bulk Na contents is also characterized by the highest $^{87}Sr/^{86}Sr$ ratio, meaning that the fluid should be characterized by $^{87}Sr/^{86}Sr < 0.705$. The Sr in the hydrothermal solution did not derived from surrounding Statherian gneissses which have probably high Sr isotopic ratio (as they are much older and have high Rb/Sr ratios); a better explanation is that the fluid originated from the basic magma itself. Mineral compositions of the eclogite TINZ 3 are best reproduced using hydrous composition in thermodynamic modelling despite the fact that the eclogitic assemblage is anhydrous. Modelled jadeite content (max. 22 mol%) of clinopyroxene are still lower than the maximum measured (26 mol%). It is probable that dehydration-controlled loss of alkalies during HP crystallization subsequently played a minor role in modifying the bulk composition of the eclogite and garnet amphibolites.

5.3. Significance of the U–Pb zircon age

According to previous studies on zircon in high pressure rocks, this phase can develop at three different stages (see Rubatto et al., 1999; Hermann et al., 2001): (i) during crystallization of the igneous precursor, (ii) during prograde or peak eclogitic metamorphism, (iii) during retrograde metamorphic evolution. The proxies used to determine its crystallization history are the internal structure of the grains, its textural setting and the trace-element chemistry (mainly Th/U ratios and REE patterns). Because of the small size of zircons, it was not possible to analyze their REE composition after ablation for geochronological purposes.

Zircons from the eclogite TINZ 3 are homogeneous without oscillatory zoning (Fig. 11). They are characterized by very low Th/U ratios (<0.1 with two spots at 0.3; Table 3) which is a typical fingerprint of metamorphic growth (Rubatto, 2002). The zircons are found in the omphacitic matrix and, in a few cases, as inclusions into garnet rims (Fig. 11). TINZ 3 shows minor development of retrograde minerals but the zircons are systematically found in microdomains with amphibole and/or ilmenite (Fig. 11). Previous studies dealing with zircon dating on thin sections from Dabie Shan eclogites have properly shown, using both geochemical and textural evidences, that zircons included in the core of garnet recorded prograde or peak HP metamorphic ages while those in garnet rims, in the matrix or in retrograde microdomains formed at higher temperature, recorded younger exhumation stages (Gao et al., 2011; Zhou et al., 2011). According to the fixed composition phase diagram, development of amphibole and especially ilmenite requires low pressure (<10 kbar) and temperature around 650–750 °C (see Fig. 14). Ilmenite formed during the retrograde path of the metamorphic evolution; the close spatial relationships between rutile, ilmenite and zircon suggest that the latter formed during the rutile to ilmenite transition where rutile acted as the main source for Zr. Fe–Ti oxide are indeed the main source of Zr during metamorphic reactions (Bingen et al., 2001). Zircon formed in the amphibolite facies (i.e. in the presence of plagioclase) should have a different REE composition than eclogitic zircon but, as said above, because of their small size, it was not possible to characterize their trace-element chemistry.

The oldest $^{39}Ar–^{40}Ar$ ages obtained on phengite from high-pressure metasediments at Tidéridjaouine is 620 ± 3 Ma (Caby and Monié, 2003), and it undoubtedly represents a cooling age

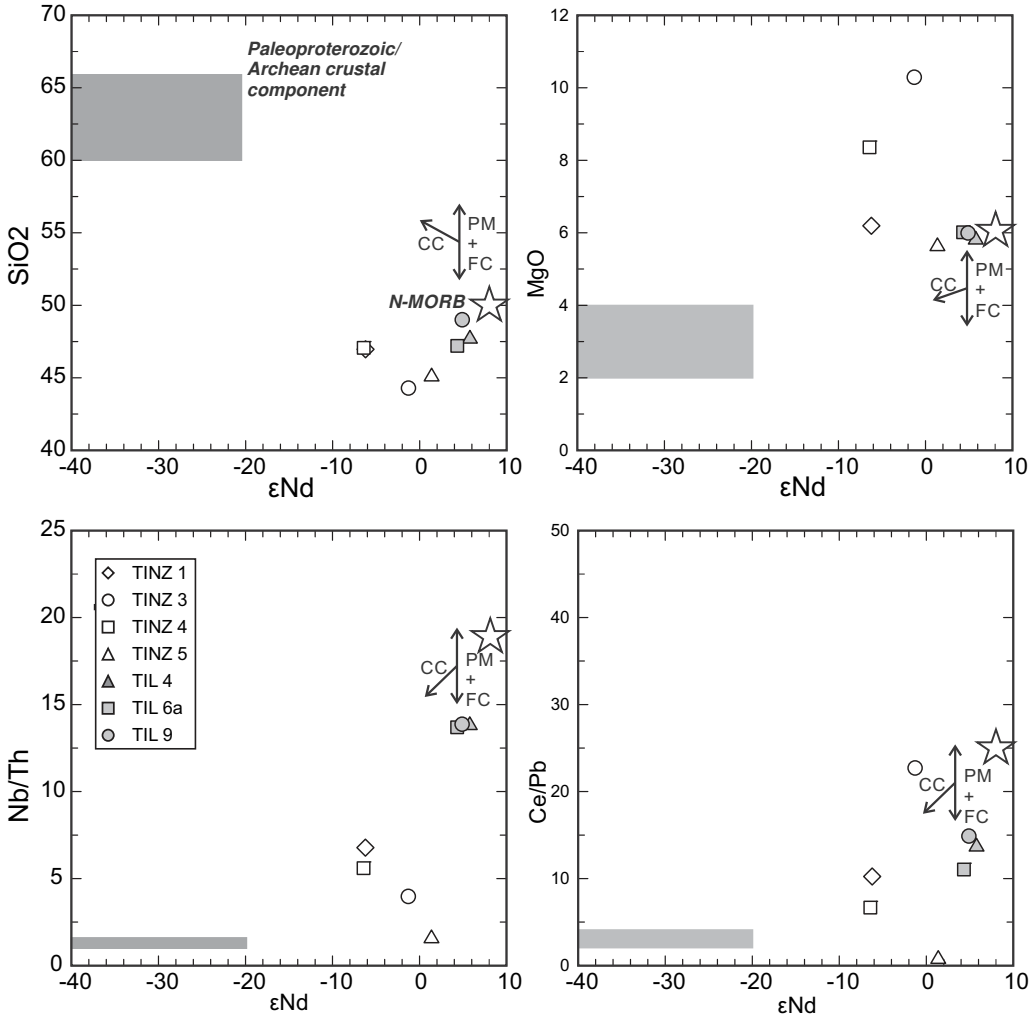

Fig. 15. Variation of some geochemical parameters with the initial ε_{Nd}. CC: crustal contamination trend representing assimilation and source contamination; PM: partial melting trend; FC: fractional crystallization trend. Isotopic data from Ait-Djafer et al. (2003) together with trace-element data of the upper crust (Rudnick and Gao, 2003) were chosen for the crustal contaminant. N-MORB data from Workman and Hart (2005) and Hofmann (1988).

according to the low closure temperature of the K–Ar system in phengite (<500 °C; Bosse et al., 2005). The similar values obtained by U–Pb zircon (for which closure temperature are >900 °C, Cherniak and Watson, 2001) and ^{39}Ar–^{40}Ar dating also support that zircon grew during a rapid exhumation of HP units (from 900° to 500 °C within error limits, i.e. 3 Myrs), probably after the thermal peak in the *P*–*T* path.

5.4. Nature, source and tectonic setting of the igneous precursors

5.4.1. Alkaline and tholeiitic affinities

Geochemical data show that the eclogites and garnet amphibolites represent former metabasalts with smooth REE patterns and high contents in very incompatible elements (Zr, Nb, LREE, Th) (Fig. 10). TINZ 5 is however a former cumulate gabbro as attested by the high Sr, Eu/Eu* and Al values. The TAS and AFM diagrams should be interpreted with caution here as alkalis were depleted in some samples during late to post-magmatic alteration. Samples with no negative anomalies in K (and hence, not depleted in alkalis) plot in the subalkaline and tholeiitic fields of these two diagrams. Based on generally immobile major and trace-elements, most samples plot in the tholeiitic field, except TINZ 3 which has the immobile element pattern of an alkali basalt (Fig. 9). The latter however shows the most pronounced negative K peak indicating that it has been strongly depleted in alkalies after igneous emplacement. Coexistence of alkaline and tholeiitic samples can be easily explained by different degrees of partial melting in the mantle source. TINZ 3 is indeed strongly enriched in very incompatible elements (Zr, Th, Nb...) compared to other samples and it also shows the highest high La/Sm ratio. Although partial melting and differentiation plays a crucial role on major and trace-element composition of igneous precursors, the heterogeneous isotopic signatures also argue for variable crustal contribution during their genesis.

5.4.2. An enriched and heterogeneous subcontinental lithospheric mantle source for basaltic precursors

The $(Nb/Th)_N$ ratio (a proxy for the Nb anomaly) is high for Tiléouine sample (0.7) compared to arc basalts (usually <0.1) while Tidéridjaouine samples have variable ratios (0.08–0.36) but still higher than arc basalts. The poorly developed negative Nb anomaly (Fig. 10) does not agree with a supra-subduction origin. All samples show enrichment in LREE compared to HREE with high average contents in incompatible elements relative to MORBs. There is also a negative correlation between $^{87}Sr/^{86}Sr$ initial ratios and ε_{Nd} from 0.706, +6 to 0.717, −6 (Fig. 13); the Tileouine samples plot close to the DMM at 700 Ma while the Tideridjaouine eclogite and amphibolites are trending toward an old crustal component here represented by the In Ouzzal Archean and Paleoproterozoic rocks

(Ait-Djafer et al., 2003; Fig. 13). Ratios of very incompatible trace-elements such as Ce/Pb and Nb/Th (less sensitive to partial melting and differentiation degrees compared to elemental abundances) are also lower in the Tideridjaouine samples and correlate with a decrease in ε_{Nd} values (Fig. 14), arguing for a significant crustal signature in these samples.

This crustal component can originate from two ways: it can be assimilation during emplacement in the crust of mantle-derived precursor basalts or it can represent a mix between a depleted mantle component and old radiogenic recycled crustal components in the source itself of the precursor basalts. As there is no comprehensive geochemical and isotopic study on the Tassendjanet samples, the crustal component was represented by the mean upper continental crust (UCC) for concentrations and Archean/Paleoproterozic In Ouzzal rocks for age-corrected isotopic signatures (Fig. 14). If the source contamination model is considered (mix between DMM and UCC), the most radiogenic metabasalts can be explained by the presence of 0.1–2 wt% of recycled crustal component in the mantle (Fig. 13). Crustal assimilation would, on the other hand, require more than 30 wt% of crustal material to be mixed with fresh mantle-derived basalt to explain the isotopic composition of TINZ 4. This is a consequence of the very different Sr and Nd concentrations in the mantle and in basalts. The latter being much richer, a much higher contribution from the crust is required.

Adding 30% of felsic crustal material (~70 wt% SiO_2) to a basalt (~50 wt%SiO_2) would lead to a mixed magma with 56 wt% SiO_2. About 2% crustal contamination in the mantle source (~40 wt% SiO_2) will only lead to a slight increase of SiO_2 in the mantle source (40.6 wt%) and it will not modify significantly the partial melt major element composition. The same conclusion arises for incompatible trace-elements and other major elements. The silica or MgO vs ε_{Nd} plot of Fig. 14 does not show a negative correlation that would support crustal assimilation. Moreover, the sample with the most radiogenic signatures (TINZ 4) has low incompatible elements contents (Fig. 10) and this cannot be explained by crustal assimilation. All these observations and qualitative estimations argue for the generation of the basaltic precursor from an enriched mantle source, representing a mix between depleted components and recycled crustal components. Nd T_{DM} model ages are around 800 Ma for Tiléouine samples and down to 2.0 Ga for the Tidéridjaouine ones, the crustal component is thus probably of Paleoproterozoic or Archean age. Such enriched and heterogeneous signatures are typical of the subcontinental lithospheric mantle (Xu et al., 2008; Griffin et al., 2009).

Juvenile CAMP continental tholeiites from Guyana characterized by the same isotopic compositions ($^{87}Sr/^{86}Sr$: 0.703–0.705, ε_{Nd}: +5 to +6) and very similar trace-element distribution compared to Tileouine samples are interpreted as subcontinental mantle melts, with a source composition close to DMM but contaminated by an enriched mantle component (EM) (Deckart et al., 2005).

5.4.3. *Emplacement in the shoulder of a Neoproterozoic continental rift*

The association of continental tholeiitic and alkaline basalts is characteristic of an intraplate setting, especially rifts. Tidéridjaouine and Tiléouine samples have similar immobile major and trace-element distribution than the Dead Sea rift and CAMP basalts (Figs. 9, 10 and 16). TINZ 5 is outside the field of rift basalts in Fig. 16 but this sample is a former cumulate and cannot be directly compared to volcanic rocks. TINZ 3 is also outside the field of rift basalts in the Th/Yb vs La/Sm plot (Fig. 16), it is trending toward the value of mean upper continental crust. According to the more radiogenic Sr and Nd isotopic composition, this shift reflects a contamination by an old crust. Jurassic CAMP basalts were formed during the breakup of Pangea and were emplaced around the margin of the Central Atlantic Ocean. By analogy with the CAMP, the basaltic precursors

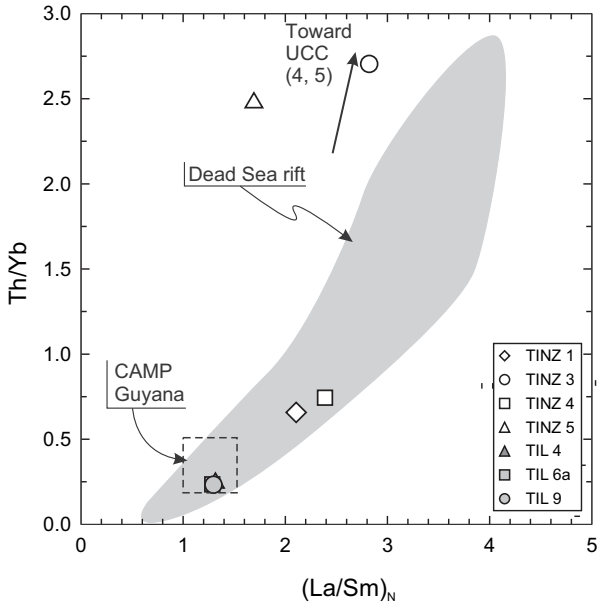

Fig. 16. Comparison between the Dead Sea rift basalts (data from the online GEOROC database) and samples from the Tassendjanet area. CAMP values are from Deckart et al. (2005). Upper continental crust values (Th/Yb = 5; $(La/Sm)_N$ = 4) calculated from the data of Rudnick and Gao (2003).

of the eclogites and amphibolites were probably emplaced along the shoulders of a Neoproterozoic continental rift, evolving toward a true oceanic basin (as for the CAMP magmas). The association of tholeiitic basalts with alkaline lavas is indeed typical of rifting stages (Alici et al., 2001; see Fig. 9) and also characterizes the Central Atlantic Magmatic province (Marzoli et al., 1999; McHone, 2000). Here, the rift stage would have a maximum age of 800 Ma, based on Nd T_{DM} model ages of the studied rocks.

5.5. *A tentative geodynamic scenario for HP metamorphism in the Tassendjanet-Tidéridjaouine terrane (Fig. 17)*

The continental origin of the eclogite and garnet amphibolites is clearly assessed both by their geochemical signature and by their association with high-pressure aluminous garnet-kyanite-phengite metasediments (Caby and Monié, 2003). Geochemical fingerprints of the basaltic precursors share many similarities with rift-related basalts, especially with the CAMP Jurassic basalts (Figs. 9, 10 and 16). The Neoproterozoic model ages of the Tiléouine samples argue for an emplacement after 800 Ma and their geochemistry points to an emplacement along the continental shoulder of an oceanic basin (Fig. 17, stage 1).

The subduction of a light continental passive margin requires that it is pulled down by a dense oceanic lithosphere (Ernst, 2001). Its existence is indirectly suggested by the presence of rift-like metabasalts (Fig. 17, stage 1). True ophiolitic assemblages have not been recognized yet in the Tassendjanet but large pre-metamorphic mafic-ultramafic complexes formed by serpentinite, amphibolite and talc-rich schists have been mapped (Figs. 1 and 2a) and could be good candidates for oceanic crust and mantle. Subduction of oceanic lithosphere leads to the formation of supra-subduction arc systems. It is difficult to locate such an arc in the area of interest. It is however important to notice that Neoproterozoic turbiditic greywackes of the "Série Verte" that derive from the erosion of mainly andesitic volcanics are cut by numerous subduction-related calc-alkaline magmas (tonalite-diorite-granodiorite hypovolcanic stocks), whereas the same type of plutonic rocks are reworked as pebbles in the pebbly greywackes ("autocanibalistic development",

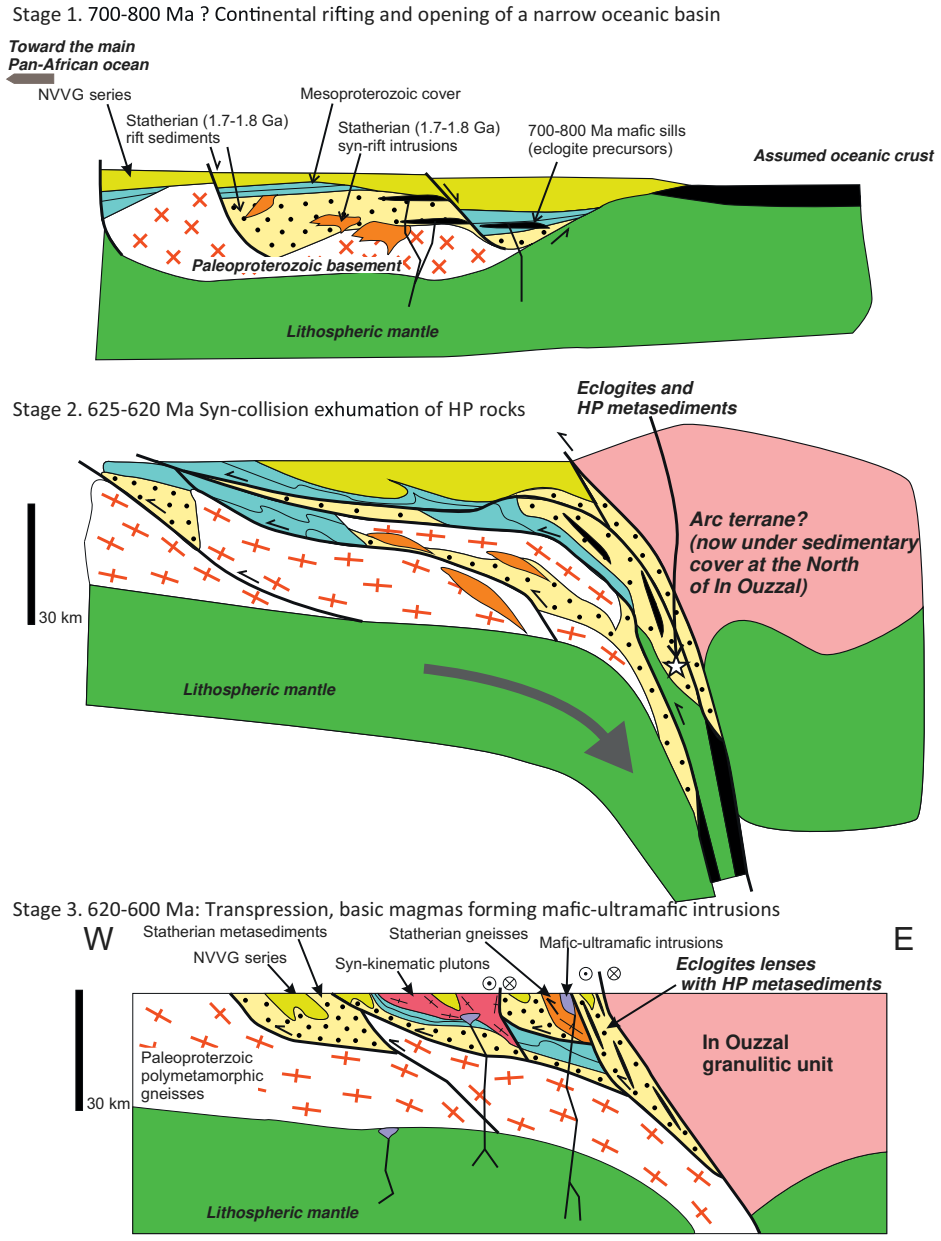

Fig. 17. Interpretative sketch summarizing the geodynamic evolution of the Tassendjanet-Tidéridjaouine terrane deduced from data collected on eclogite and garnet amphibolites.

Caby et al., 1977). The post-collisional northward movement of the In Ouzzal terrane, located east of the suture zone, is at least of 150 km (and possibly much more if we consider that it was adjacent to the Iforas granulitic unit, 300 km to the south, both having probably moved together towards the north before being separated). With this configuration, possible arc relics would have been transported also toward the North and no more in their original location. The Gora Akofou andesites (Fig. 1a) lying upon the northern edge of the In Ouzzal terrane have continental arc affinities (Chikhaoui et al., 1980) and were proposed by Caby and Monié (2003) to be the remnants of the supra-subduction igneous activity. Scarce evidences of arc magmatism and/or HT-MP metamorphism typical of arcs are also found along the In Ouzzal border. It includes dispersed garnet pyroxenites at Tiléouine and the Camp Zohra arc complex (Fig. 1a) overthrusting the northern edge of the In Ouzzal terrane (Mokri et al., 2008). The granulitic garnet metagabbros are locally imprinted by low-temperature medium to high-pressure glaucophane-bearing assemblage. Again, the relationships between these objects and the Tiléouine-Tidéridjaouine eclogite are not known but we can attest that arc relics are not rare in the area. The possibility that an arc system did not developed above the slab has also to be considered. Fast subduction of a small oceanic basin does not leave enough time for a mature arc system to form. The absence of arc in the Alps has been interpreted in this way (O'Brien, 2001).

PT conditions near peak stage (650 °C–21 kbar, see Fig. 14) attest for very cold temperature-depth gradient (9 °C/km) typical of a cold passive margin subduction (see Ernst, 2001). Zircons are found within the rim of garnet, the omphacitic matrix or against ilmenite–rutile association in retrograde, amphibole bearing domains (Fig. 11). They are probably associated with the consumption of rutile to form ilmenite between 14 and 10 kbar. The 623 ± 2 Ma age (Fig. 13) thus corresponds to the exhumation stage of the eclogite, being very similar to the 620–624 Ma ages

obtained on high-pressure micaschists and eclogite in the Gourma belt (Sm–Nd mineral isochron and ^{39}Ar–^{40}Ar dating of phengites; Jahn et al., 2001). It is also in agreement, within errors, with the laser ^{39}Ar–^{40}Ar dating on phengites from high-pressure metasediments from Tidéridjaouine (620 ± 3 Ma; Caby and Monié, 2003). All these ages represent closure cooling ages that are here interpreted as dating the exhumation. This process of exhumation is associated with west-verging recumbent to sheath folds and down-dip lineations (Caby and Monié, 2003). The subducting slab was therefore dipping toward the east (Fig. 17, stage 2). According to structural observations, the exhumation of high-pressure units was syn-collisional, as for many continental HP to UHP units (Chopin, 2003).

Retrogressed eclogites sampled at Tiléouine are embedded in deformed orthogneiss developing an horizontal lineation. The latter is outlined by biotite and has thus been acquired in medium-pressure, medium temperature conditions during the sinistral strike-slip lateral movement along the West-Ouzzalian shear zone. The northward motion of the In Ouzzal granulitic unit forming mylonites is not dated. Ferkous and Monié (2002) dated an igneous gabbro within the East Ouzzalian shear zone at 623–613 Ma (^{39}Ar–^{40}Ar on amphibole and biotite) and a hornblende from a mylonite showing strong zoning with ^{39}Ar–^{40}Ar laser ages from 849 Ma in the core to 626 Ma in the recrystallized rims. All these Ar–Ar ages show inheritance patterns and the tectonic significance of these ages is not clear. If we extrapolate these results to the West Ouzzalian shear zone, it means that the transpressive tectonics started just after the exhumation of the eclogites (Fig. 17, stage 3). The lateral movements lasted at least until 592 Ma as it affects the Tin Zebane alkaline dyke swarm (Hadj-Kaddour et al., 1998). This period was also marked by emplacement of granitic bodies, mafic plutons and by localized high-temperature metamorphism (Bosch et al., 2002; Liégeois et al., 1998, 2003; Caby and Monié, 2003).

6. Conclusions

Fresh and retrogressed eclogites from the Tassendjanet and Tidéridjaouine areas in Western Hoggar recorded peak *P*–*T* conditions around 650 °C and 20–22 kbar. The exhumation path is characterized by a slight increase of temperature, max. 730 °C at 14–18 kbar and then by cooling to 610° C and 7–10 kbar. According to geochemical and isotopic signature of the eclogite and garnet amphibolites, their igneous precursors are former intrusions in the shoulder of a continental rift that most probably evolved towards a true oceanic basin. The source of the rift metabasalts is a heterogeneous subcontinental lithospheric mantle variously contaminated by recycled (>1.8 Ga)crustal material. Emplacement of these rift basalts occurred in the Neoproterozoic for most samples, probably around 700–800 Ma according to Nd T_{DM} model ages. Fragment of oceanic lithosphere have not been recognized yet in the area but good candidates preserved as pre-metamorphic mafic-ultramafic complexes exist in the Tassendjanet terrane. Relicsof supra-subduction arc systems are numerous but the post-collisional northward movement of the In Ouzzal terrane located to the east of the HP units could have led to the northward tectonic transport of these arc relics relative to their original accreted position. Another possibility is that an arc system did not develop; this could happen when the oceanic subduction is short-lived.

Metamorphic zircons in the fresh eclogite sample crystallized in the vicinity of rutile and ilmenite in retrograde amphibole-bearing domains. U–Pb dating of these zircons by LA–ICP–MS directly on the thin section gave an age of 623 ± 2 Ma which is interpreted as representing the exhumation of the HP units in the Tassendjanet terrane. This exhumation is related to a westward transport of HP units meaning that the subducting slab was dipping eastward. Syn-collisional exhumation was probably rapidly (within a few million years) followed by transpressive shearing along the suture zone linked to the northward movement of the In Ouzzal terrane. Sinistral strike-slip shearing in the Tassendjanet-Tidéridjaouine area probably began as soon as 620 Ma but geochronological data are still needed to constrain the timing of northward motion of the In Ouzzal terrane and the time laps between syn-collisional and post-collisional tectonics.

Acknowledgments

The fantastic 2005 fieldtrip in the Western Hoggar would not have been possible without the enthusiastic support of the "Centre de Recherche en Astronomie, Astrophysique et Géophysique" (CRAAG), USTHB fellows (Safouane Djemai, Saïda Aït-Djafer, Amar Drareni and Zouhir Adjerid), Gaston Godard (Institut de Physique du Globe, Paris) and the team of Tuareg drivers. Patricia Hermand and Christine Gilson (Royal Museum for Central Africa) are thanked for their precious help on Sr–Nd isotopic analysis. We acknowledge the three anonymous reviewers for their insightful comments.

Appendix A. Analytical appendix

Major element composition of minerals was determined with an electron probe micro-analyser (EPMA) at the CAMPARIS service (University of Paris VI France). The probe was a Cameca SX100 equipped with four wavelength-dispersive and one energy-dispersive spectrometer. Diffracting crystals were LTAP for Na and Mg; TAP for Si and Al; LPET for K, Ca and Cr; LLIF for Ti, Mn and Fe. The operating conditions involve a beam energy of 15 keV, a current of 10 nA and a beam diameter of ~1 μm. Counting times were fixed to 20 s for peaks and 10 s for backgrounds on each side of the peak. Calibration was set up with natural and artificial silicates and oxides. Reduction of raw data was processed using the PAP model (Pouchou and Pichoir, 1991) integrated in the Cameca software package. Composition of clinopyroxene, amphibole, plagioclase and garnet are presented as Supplementary material B.

For major and trace-element analyses, sample powders were digested using the alkali fusion method: 0.3 g of sample has been mixed to 0.9 g of lithium metaborate and heated during 2 h at 1000 °C. The fused beads were dissolved in 2% nitric acid. Major elements have been determined with an ICP-AES (Royal Museum for Central Africa, Belgium) and the calibration method used 7 natural standards; trace elements have been dosed by ICP–MS on a VG Plasmaquad 2+ (Royal Museum for Central Africa, Belgium) using a set of artificial and natural standards.

The analyses of Sr and Nd isotopic composition were carried out on a thermal-ionization mass spectrometer (VG sector 54) hosted by both the Royal Museum for Central Africa and the Université Libre de Bruxelles (Belgium). Sr and Nd were isolated using conventional cation exchange chromatography (Pin et al., 1994) after a HF-HFNO_3-HCl digestion.

U–Pb dating on zircon was performed on the thin section of TINZ 3 by LA-SF-ICP-MS at Geosciences Montpellier (France). The instruments were a Lambda Physik CompEx 102 excimer laser generating 15 ns duration pulses of radiation at a wavelength of 193 nm and a ThermoFinnigan Element XR high resolution (HR–) ICP–MS. Data were acquired at low resolution ($\Delta M/M = 300$) in the fast electrostatic scan mode. Signals were acquired in pulse counting mode using 3 points per peaks and a 20% mass window. A pre-ablation step consisting of 7 pulses with a beam diameter of 26 μm was applied to clean the sample surface. Then the acquisition step began with 15 s of gas blank measurement followed by 230 pulses of laser ablation at a frequency of 5 Hz with a spot size of 15 μm (about 45 s of data acquisition). Measured isotopic ratios were monitored with reference to the G91500 zircon standard with a $^{206}Pb/^{238}U$

ratio of 0.17917 and a $^{207}Pb/^{206}Pb$ ratio of 0.07488 equivalent to ages of 1062 Ma and 1065 Ma, respectively. The standard was measured four times each five unknowns in a sequence of 2 standards, 5 unknowns and 2 standards (see Bosch et al., 2011 for details).

References

Agard, P., Yamato, P., Jolivet, L., Burov, E., 2009. Exhumation of oceanic blueschists and eclogites in subduction zones: timing and mechanisms. Earth-Science Reviews 92, 53–79.

Agbossoumondé, Y., Ménot, R.P., Guillot, S., 2001. Metamorphic evolution of Neoproterozoic eclogites from south Togo (West Africa). Journal of African Earth Sciences 33, 227–244.

Ait-Djafer, S., Ouzegane, K., Liégeois, J.-P., Kiénast, J.R., 2003. An example of post-collisional mafic magmatism: the gabbro-anorthosite layered complex from the Tin Zebane area (western Hoggar, Algeria). Journal of African Earth Sciences 37, 313–330.

Alici, P., Temel, A., Gourgaud, A., Vidal, P., Gündogdu, M.N., 2001. Quaternary Tholeiitic to alkaline volcanism in the Karasu Valley, Dead Sea Rift Zone, Southeast Turkey: Sr-Nd-Pb-O isotopic and trace-element approaches to crust-mantle interaction. International Geology Review 43, 120–138.

Allègre, C.J., Caby, R., 1972. Chronologie absolue du Précambrien de l'Ahaggar occidental. Comptes Rendus Académie Sciences Paris 275, 1095–1098.

Bernard-Griffiths, J., Peucat, J.J., Ménot, R.P., 1991. Isotopic (Rb-Sr, U-Pb and Sm-Nd) and trace-element geochemistry of eclogites from the Pan-African Belt – a case-study of Ree fractionation during high-grade metamorphism. Lithos 27, 43–57.

Bingen, B., Austhreim, H., Whitehouse, M., 2001. Ilmenite as a source for zirconium during high-grade metamorphism?Textural evidence from the caledonides of Western Norway and implications for zircon geochronology. Journal of Petrology 42, 355–375.

Bittam-Derridj, A., Ouzegane, K., Adjerid, Z., Godard, G., Kiénast, J.-R., 2010. Les éclogites granulitisées de Ti-N-Eggoleh (terrane du Serouenout, Hoggar Central): etude métamorphique et consequence géodynamique. Bulletin du Service Géologique National d'Algérie 21, 117–136.

Black, R., Latouche, L., Liégeois, J.P., Caby, R., Bertrand, J.M., 1994. Pan-African displaced terranes in the Tuareg Shield (Central Sahara). Geology 22, 641–644.

Boniface, N., Schenk, V., 2012. Neoproterozoic eclogites in the Paleoproterozoic Ubendian Belt of Tanzania: Evidence for a Pan-African suture between the Bangweulu Block and the Tanzania Craton. Precambrian Research 208–211, 72–89.

Bosch, D., Hammor, D., Bruguier, O., Caby, R., Luck, J.M., 2002. Monazite "in situ" Pb-207/Pb-206 geochronology using a small geometry high-resolution ion probe.Application to Archaean and Proterozoic rocks. Chemical Geology 184, 151–165.

Bosch, D., Garrido, C.J., Bruguier, O., Dhuime, B., Bodinier, J.L., Padròn-Navarta, J.A., Galland, B., 2011. Building an island-arc crustal section: time constraints from a LA-ICP-MS zircon study. Earth and Planetary Science Letters 309, 268–279.

Bosse, V., Féraud, G., Ballèvre, M., Peucat, J.-J., Corsini, M., 2005. Rb-Sr and $^{40}Ar/^{39}Ar$ ages in blueschists from the Ile de Groix (Armorican Massif, France): Implications for closure mechanisms in isotopic systems. Chemical Geology 220, 21–45.

Burov, E., Jolivet, L., Le Pourhiet, L., Poliakov, A., 2001. A thermomechanical model of exhumation of high pressure (HP) and ultra-high pressure (UHP) metamorphic rocks in Alpine-type collision belts. Tectonophysics 342, 113–136.

Caby, R., 1969. La Chaîne pharusienne dans le Nord-Ouest de l'Ahaggar (Sahara central, Algérie); sa place dans l'orogenèse du Précambrian supérieur en Afrique. Unpublished PhD Thesis. Univ. Montpellier, 335 pp.

Caby, R., 1996. A review of the in Ouzzal granulitic terrane (Tuareg shield, Algeria): its significance within the Pan-African Trans-Saharan belt. Journal of Metamorphic Geology 14, 659–666.

Caby, R., 2003. Terrane assembly and geodynamic evolution of central-western Hoggar: a synthesis. Journal of African Earth Sciences 37, 133–159.

Caby, R., Dostal, J., Dupuy, C., 1977. Upper Proterozoic volcanic graywackes from northwestern Hoggar (Algeria); geology and geochemistry. Precambrian Research 5, 283–297.

Caby, R., Andreopoulos-Renaud, U., 1983. 1800 Ma age of sub-alkaline magmatism associated with monocyclic metasediments of the Pan-African Belt of the central Sahara. Journal of African Earth Sciences 1, 193–197.

Caby, R., Monié, P., 2003. Neoproterozoic subductions and differential exhumation of western Hoggar (southwest Algeria): new structural, petrological and geochronological evidence. Journal of African Earth Sciences 37, 269–293.

Carswell, D.A., Zhang, R.Y., 1999. Petrographic characteristics and metamorphic evolution of ultrahigh-pressure eclogites in plate-collision belts. International Geology Review 41, 781–798.

Cawood, P.A., Kroner, A., Pisarevsky, S., 2006. Precambrian plate tectonics: criteria and evidence. GSA Today 16, 4–11.

Champenois, M., Boullier, A.M., Sautter, V., Wright, L.I., Barbey, P., 1987. Tectonometamorphic evolution of the gneissic Kidal assemblage related to the Pan-African thrust tectonics (Adrar-Des-Iforas, Mali). Journal of African Earth Sciences 6, 19–27.

Chemenda, A.I., Mattauer, M., Bokun, A.N., 1996. Continental subduction and a mechanism for exhumation of high-pressure metamorphic rocks: new modelling and field data from Oman. Earth and Planetary Science Letters 143, 173–182.

Cherniak, D.J., Watson, E.B., 2001. Pb diffusion in zircon. Chemical Geology 172, 5–24.

Chikhaoui, M., Dupuy, C., Dostal, J., 1978. Geochemistry of late proterozoic volcanic rocks from Tassendjanet area (N.W. Hoggar, Algeria). Contributions to Mineralogy and Petrology 66, 157–164.

Chikhaoui, M., Dupuy, C., Dostal, J., 1980. Geochemistry and petrogenesis of late Proterozoic volcanic rocks from northwestern Africa. Contributions to Mineralogy and Petrology 73, 375–388.

Chopin, C., 2003. Ultrahigh-pressure metamorphism: tracing continental crust into the mantle. Earth and Planetary Science Letters 212, 1–14.

Clark, C., Fitzsimons, I.C.W., Healy, D., Harley, S.L., 2011. How does the continental crust get really hot? Elements 7, 235–240.

Connolly, J.A.D., 2005. Computation of phase equilibria by linear programming: a tool for geodynamic modeling and its application to subduction zone decarbonation. Earth and Planetary Science Letters 236, 524–541.

Connolly, J.A.D., 2009. The geodynamic equation of state: what and how. Geochemistry, Geophysics, Geosystems 10, q10014.

Deckart, K., Bertrand, H., Liégeois, J.P., 2005. Geochemistry and Sr, Nd,Pb isotopic composition of the Central Atlantic Magmatic Province (CAMP) in Guyana and Guinea. Lithos 82, 289–314.

Dhuime, B., Bosch, D., Bruguier, O., Caby, R., Pourtales, S., 2007. Age, provenance and post-deposition metamorphic overprint of detrital zircons from the Nathorst Land group (NE Greenland)—a LA-ICP-MS and SIMS study. Precambrian Research 155, 24–46.

Diener, J.F.A., Powell, R., White, R.W., Holland, T.J.B., 2007. A new thermo-dynamic model for clino- and orthoamphiboles in Na_2O-CaO-FeO-MgO-Al_2O_3-SiO_2-H_2O-O. Journal of Metamorphic Geology 25, 631–656.

Dostal, J., Caby, R., Dupuy, C., 1979. Metamorphosed alkaline intrusions and dyke complexes within the Pan-African Belt of western Hoggar (Algeria): geology and geochemistry. Precambrian Research 10, 1–20.

Dostal, J., Caby, R., Dupuy, C., Mevel, C., Owen, J.V., 1996. Inception and demise of a Neoproterozoic ocean basin: evidence from the Ougda complex, western Hoggar (Algeria). Geologische Rundschau 85, 619–631.

Duretz, T., Gerya, T.V., Kaus, B.J.P., Andersen, T.B., 2012. Thermomechanical modeling of slab eduction. Journal of Geophysical Research: Solid Earth 117, B08411.

Ernst, W.G., 2001. Subduction, ultrahigh-pressure metamorphism, and regurgitation of buoyant crustal slices – implications for arcs and continental growth. Physics of the Earth and Planetary Interiors 127, 253–275.

Ernst, W.G., Maruyama, S., Wallis, S., 1997. Buoyancy-driven, rapid exhumation of ultrahigh-pressure metamorphosed continental crust. Proceedings of the National Academy of Sciences of the United States of America 94, 9532–9537.

Ferkous, K., Monié, P., 2002. Neoproterozoic shearing and auriferous hydrothermalism along the lithospheric N–S East In Ouzzal shear zone (Western Hoggar, Algeria, North Africa). Journal of African Earth Sciences 35, 399–415.

Ganne, J., De Andrade, V., Weinberg, R.F., Vidal, O., Dubacq, B., Kagambega, N., Naba, S., Baratoux, L., Jessell, M., Allibon, J., 2012. Modern-style plate subduction preserved in the Palaeoproterozoic West African craton. Nature Geoscience 5, 60–65.

Gao, X.Y., Zheng, Y.F., Chen, Y.X., 2011. U–Pb ages and trace elements in metamorphic zircon and titanite from UHP eclogite in the Dabie orogen: constraints on *P–T–t* path. Journal of Metamorphic Geology 29, 721–740.

Gerya, T.V., Stöckhert, B., Perchuk, A.L., 2002. Exhumation of high-pressure metamorphic rocks in a subduction channel: a numerical simulation. Tectonics 21, 1056.

Guillot, S., Hattori, K., Agard, P., Schwartz, S., Vidal, O., 2009. Exhumation processes in oceanic and continental subduction contexts: a review. In: Lallemand, S., Funiciello, F. (Eds.), Subduction Zone Geodynamics. Springer, Berlin/Heidelberg, pp. 175–205.

Green, E.C.R., Holland, T.J.B., Powell, R., 2007. An order-disorder model foromphacitic pyroxenes in the system jadeite–-hedenbergite-acmite, with applications to eclogite rocks. American Mineralogist 92, 1181–1189.

Griffin, W.L., O'Reilly, S.Y., Afonso, J.C., Begg, G.C., 2009. The composition and evolution of lithospheric mantle: a re-evaluation and its tectonic implications. Journal of Petrology 50, 1185–1204.

Hadj-Kaddour, Z., Liégeois, J.P., Demaiffe, D., Caby, R., 1998. The alkaline-peralkaline granitic post-collisional Tin Zebane dyke swarm (Pan-African Tuareg shield, Algeria): prevalent mantle signature and late agpaitic differentiation. Lithos 45, 223–243.

Haddoum, H., Guiraud, R., Moussine-Pouchkine, A., 2001. Hercynian compressional deformations of the Ahnet–Mouydir Basin, Algerian Saharan Platform: far-field stress effects of the Late Palaeozoic orogeny. Terra Nova 13, 220–226.

Hermann, J., Rubatto, D., Korsakov, A., Shatsky, V., 2001. Multiple zircon growth during fast exhumation of diamondiferous, deeply subducted continental crust (Kokchetav Massif, Kazakhstan). Contributions to Mineralogy and Petrology 141, 66–82.

Hofmann, A.W., 1988. Chemical differentiation of the Earth – the relationship between mantle, continental-crust, and oceanic-crust. Earth and Planetary Science Letters 90, 297–314.

Holland, T.J.B., Blundy, J., 1994. Nonideal interactions in calcic amphiboles and their bearing on amphibole-plagioclase thermometry. Contributions to Mineralogy and Petrology 116, 433–447.
Holland, T.J.B., Powell, R., 1998. An internally consistent thermodynamic data set for phases of petrological interest. Journal of Metamorphic Geology 16, 309–343.
Holland, T.J.B., Powell, R., 2003. Activity-composition relations for phases in petrological calculations: an asymmetric multicomponent formulation. Contributions to Mineralogy and Petrology 145, 492–501.
Jahn, B., Caby, R., Monié, P., 2001. The oldest UHP eclogites of the World: age of UHP metamorphism, nature of protoliths and tectonic implications. Chemical Geology 178, 143–158.
John, T., Schenk, V., Haase, K., Scherer, E., Tembo, F., 2003. Evidence for a Neoproterozoic ocean in south-central Africa from mid-oceanic-ridge–type geochemical signatures and pressure-temperature estimates of Zambian eclogites. Geology 31, 243–246.
Kohn, M.J., Spear, F.S., 1990. Two new geobarometers for garnet amphibolites, with applications to Southeastern Vermont. American Mineralogist 75, 89–96.
Labrousse, L., Jolivet, L., Agard, P., Hébert, R., Andersen, T.B., 2002. Crustal-scale boudinage and migmatization of gneiss during their exhumation in the UHP Province of Western Norway. Terra Nova 14, 263–270.
Leake, B.E., Woolley, A.R., Arps, C.E.S., Birch, W.D., Gilbert, M.C., Grice, J.D., Hawthorne, F.C., Kato, A., Kisch, H.J., Krivovichev, V.G., Linthout, K., Laird, J., Mandarino, J.A., Maresch, W.V., Nickel, E.H., Rock, N.M.S., Schumacher, J.C., Smith, D.C., Stephenson, N.C.N., Ungaretti, L., Whittaker, E.J.W., Youzhi, G., 1997. Nomenclature of amphiboles: report of the subcommittee on amphiboles of the international mineralogical association, commission on new minerals and mineral names. American Mineralogist 82, 1019–1037.
Liégeois, J.P., Navez, J., Hertogen, J., Black, R., 1998. Contrasting origin of post-collisional high-K calc-alkaline and shoshonitic versus alkaline and peralkaline granitoids. The use of sliding normalization. Lithos 45, 1–28.
Liégeois, J.P., Latouche, L., Boughrara, M., Navez, J., Guiraud, M., 2003. The LATEA metacraton (Central Hoggar, Tuareg shield, Algeria): behaviour of an old passive margin during the Pan-African orogeny. Journal of African Earth Sciences 37, 161–190.
Marzoli, A., Renne, P.R., Piccirillo, E.M., Ernesto, M., Bellieni, G., Min, A.D., 1999. Extensive 200-Million-year-old continental flood basalts of the Central Atlantic Magmatic Province. Science 284, 616–618.
McDonough, W.F., Sun, S.S., 1995. The composition of the Earth. Chemical Geology 120, 223–253.
McHone, J.G., 2000. Non-plume magmatism and rifting during the opening of the central Atlantic Ocean. Tectonophysics 316, 287–296.
Mints, M.V., Belousova, E.A., Konilov, A.N., Natapov, L.M., Shchipansky, A.A., Griffin, W.L., O'Reilly, S.Y., Dokukina, K.A., Kaulina, T.V., 2010. Mesoarchean subduction processes: 2.87 Ga eclogites from the Kola Peninsula, Russia. Geology 38, 739–742.
Mokri, M., Ouzegane, K., Haddoum, H., Kienast, J.R., Liégeois, J.P., 2008. Le complexe mafique et ultramafique du terrane de l'Ahnet, Hoggar occidental: structure, pétrologie et géochimie. In: 22th Colloquium of African Geology, Tunis, Tunisia, pp. 366–367.
Moussine-Pouchkine, A., Bertrand-Sarfati, J., Ball, E., Caby, R., 1988. Proterozoic anorogenic volcanic and sedimentary series in the Pan-African chain – the Adrar-Ahnet region (Nw Hoggar, Algeria). Journal of African Earth Sciences 7, 57–75.
Miyashiro, A., 1974. Volcanic rock series in island arcs and active continental margins. American Journal of Science 274, 321–355.
Nelson, B.K., DePaolo, D.J., 1984. 1,700-Myr greenstone volcanic successions in southwestern North America and isotopic evolution of Proterozoic mantle. Nature 312, 143–146.
O'Brien, P.J., 2001. Subduction followed by collision: Alpine and Himalayan examples. Physics of the Earth and Planetary Interiors 127, 277–291.
Ouzegane, K., Kiénast, J.R., Bendaoud, A., Drareni, A., 2003. A review of Archaean and Paleoproterozoic evolution of the In Ouzzal granulitic terrane (Western Hoggar, Algeria). Journal of African Earth Sciences 37, 207–227.
Pouchou, J.L., Pichoir, F., 1991. Quantitative analysis of homogeneous or stratified microvolumes applying the model "PAP". In: Heinrich, K., Newbury, D. (Eds.), Electron Probe Quantitation. Plenum Press, New-York, pp. 31–76, ISBN 0306438240, 9780306438240.
Ravna, E.K., 2000. Distribution of Fe^{2+} and Mg between coexisting garnet and hornblende in synthetic and natural systems: an empirical calibration of the garnet-hornblende Fe–Mg geothermometer. Lithos 53, 265–277.
Rooney, A.D., Selby, D., Houzay, J.-P., Renne, P.R., 2010. Re–Os geochronology of a Mesoproterozoic sedimentary succession, Taoudeni basin, Mauritania:implications for basin-wide correlations and Re–Os organic-rich sediments systematics. Earth and Planetary Science Letters 289, 486–496.
Rougier, S., Missenard, Y., Gautheron, C., Barbarand, J., Zeyen, H., Pinna, R., Liégeois, J.P., Bonin, B., Ouabadi, A., Derder, M.E.M., Frizon de Lamotte, D., 2013. Eocene exhumation of the Tuareg Shield (Sahara, Africa). Geology 41, 615–618.
Rubatto, D., Gebauer, D., Compagnoni, R., 1999. Dating of eclogite-facies zircons: the age of Alpine metamorphism in the Sesia Lanzo Zone (Western Alps). Earth and Planetary Science Letters 167, 141–158.
Rubatto, D., 2002. Zircon trace element geochemistry: partitioning with garnet and the link between U-Pb ages and metamorphism. Chemical Geology 184, 123–138.
Rudnick, R.L., Gao, S., 2003. Composition of the continental crust. In: Roberta, L., Rudnick (Eds.), Treatise on Geochemistry, vol. 3. Elsevier, pp. 1–64.
Sautter, V., 1985. An eclogite paragenesis from the Aleksod basement, Central Hoggar, south Algeria. Chemical Geology 50, 331–347.
Stern, R.J., 2005. Evidence from ophiolites, blueschists, and ultrahigh-pressure metamorphic terranes that the modern episode of subduction tectonics began in Neoproterozoic time. Geology 33, 557–560.
White, R.W., Powell, R., Holland, T.J.B., Worley, B.A., 2000. The effect of TiO_2 and Fe_2O_3 on metapelitic assemblages at greenschist and amphibolite facies conditions: mineral equilibria calculations in the system K_2O-FeO-MgO-Al_2O_3-SiO_2-H_2O-TiO_2-Fe_2O_3. Journal of Metamorphic Geology 18, 497–511.
White, R.W., Powell, R., Holland, T.J.B., 2007. Progress relating to calculation of partial melting equilibria for metapelites. Journal of Metamorphic Geology 25, 511–527.
Winchester, J.A., Floyd, P.A., 1977. Geochemical discrimination of different magma series and their differentiation products using immobile elements. Chemical Geology 20, 325–343.
Workman, R.K., Hart, S.R., 2005. Major and trace element composition of the depleted MORB mantle (DMM). Earth and Planetary Science Letters 231, 53–72.
Xia, Q.-X., Zheng, Y.-F., Zhou, L.-G., 2008. Dehydration and melting during continental collision: constraints from element and isotope geochemistry of low-T/UHP granitic gneiss in the Dabie orogen. Chemical Geology 247, 36–65.
Xu, Y.-G., Blusztajn, J., Ma, J.-L., Suzuki, K., Liu, J.F., Hart, S.R., 2008. Late Archean to Early Proterozoic lithospheric mantle beneath the western North China craton: Sr-Nd-Os isotopes of peridotite xenoliths from Yangyuan and Fansi. Lithos 102, 25–42.
Zetoutou, S., Ouzegane, K., Boubazine, S., Kiénast, J.R., 2004. Azrou N'Fad (Central Hoggar, Algeria) one of the deepest terranes of LATEA: arguments based on *P–T* evolution in eclogite. Journal of African Earth Sciences 39, 193–200.
Zhao, Z.-F., Zheng, Y.-F., Chen, R.-X., Xia, Q.-X., Wu, Y.-B., 2007. Element mobility in mafic and felsic ultrahigh-pressure metamorphic rocks during continental collision. Geochimica Et Cosmochimica Acta 71, 5244–5266.
Zhou, L.-G., Xia, Q.-X., Zheng, Y.-F., Chen, R.-X., 2011. Multistage growth of garnet in ultrahigh-pressure eclogite during continental collision in the Dabie orogen: constrained by trace elements and U–Pb ages. Lithos 127, 101–127.